



**TECHNICAL DOCUMENT 3324**  
October 2017

## **Development of a Comb Limiter Combiner with Sub-band known Interference Cancellation**

Jia-Chi Samuel Chieh

Approved for public release.

SSC Pacific  
San Diego, CA 92152-5001

**SSC Pacific**  
**San Diego, California 92152-5001**

---

**M. K. Yokoyama, CAPT, USN**  
**Commanding Officer**

**W. R. Bonwit**  
**Executive Director**

**ADMINISTRATIVE INFORMATION**

The work described in this report was performed for the Office of Naval Research (ONR) by the Advanced Integrated Circuit Technology Branch (Code 55250) of the 55190 Networks Division (Code 55200), Space and Naval Warfare Systems Center Pacific (SSC Pacific), San Diego, CA.

Released by  
Alex G. Phipps, Head  
Advanced Integrated Circuit  
Technology Branch

Under authority of  
Phillip Juarez, Head  
55190 Networks Division

The citation of trade names and names of manufacturers is not to be construed as official government endorsement or approval of commercial products or services referenced in this report.

AVX<sup>®</sup> is a registered trademark of AVX Corporation.  
Keysight<sup>®</sup> is a registered trademark of Keysight Technologies.  
Modelithics<sup>®</sup> is a registered trademark of Modelithics.  
Agilent<sup>®</sup> is a registered trademark of Agilent Technologies  
Agilent Momentum<sup>®</sup> is a registered trademark of Agilent Technologies.  
Ansys<sup>®</sup> HFSS is a registered trademark of Ansys, Inc.  
Rogers<sup>®</sup> RO4350B<sup>™</sup> is a registered trademark of Rogers Corporation.  
ACCU-P<sup>®</sup> is a registered trademark of AVX Corporation.  
Vishay<sup>®</sup> is a registered trademark of Vishay Intertechnology, Inc.  
Cobham<sup>®</sup> is a registered trademark of Cobham plc.

## ACRONYMS

ABSF	absorptive bandstop filters
ATP	applied thin films
BAW	bulk acoustic waves
BPF	bandpass filter
BSF	bandstop filters
CW	continuous wave
CWSP	Commercial Wideband Satellite Program
DAC	digital to analog converter
DAC	digital to analog converter
DSCS	Defense Satellite Communication System
EVM	error vector magnitude
IF	intermediate frequency
LCP	liquid crystal polymer
LNA	low-noise amplifier
LTCC	low temperature co-fired ceramic
MCM	multi-chip module
MEMs	microelectromechanical-systems
NRL	Naval Research Lab
QAM	quadrature amplitude modulation
RF	radio frequencies
SAW	surface acoustic waves
SMT	surface mount technology
SOI	signal of interest
SRF	self-resonant frequencies
SRF	self-resonant frequencies
SSC Pacific	Space and Naval Warfare Systems Center Pacific
TRL	thru-reflect-line
UCSD	University of California, San Diego
UHF	ultra high frequency
WGS	wideband global satcom

## CONTENTS

<b>1. PROJECT SUMMARY .....</b>	<b>6</b>
<b>2. OVERVIEW OF TECHNICAL APPROACH .....</b>	<b>6</b>
2.1 BROADER IMPACT .....	8
2.2 OUTLOOK OF THE NEW CAPABILITIES.....	8
<b>3. PROJECT DESCRIPTION .....</b>	<b>8</b>
3.1 COCHLEA-BASED RF CHANNELIZER DESIGN .....	8
3.2 FREQUENCY AGILE ABSORPTIVE NOTCH FILTERS.....	9
3.3 INTEGRATION OF CHANNELIZER WITH FREQUENCY AGILE NOTCH FILTER.....	13
<b>4. TECHNOLOGY DEVELOPMENT IN C-BAND.....</b>	<b>15</b>
4.1 DEVELOPMENT OF COCHLEA CHANNELIZER .....	15
4.1.1 Three-Channel Design Using Lumped Capacitors.....	15
4.1.2 Five-Channel Design using Lumped Capacitors .....	18
4.1.3 Five-channel design for C-Band .....	20
4.2 ABSORPTIVE NOTCH FILTER DESIGN .....	25
4.2.1 Design based on coupled transmission lines .....	25
4.2.2 Quasi-lumped element design.....	29
4.3 INTEGRATION OF RF CHANNELIZER WITH TUNABLE NOTCH FITLER .....	34
4.4 COMPARISON WITH PHOTONIC TECHNOLOGY .....	37
<b>5. TECHNOLOGY DEVELOPMENT IN X-BAND.....</b>	<b>38</b>
5.1 DEVELOPMENT OF COCHLEA CHANNELIZER .....	39
5.2 DEVELOPMENT OF ABSORPTIVE BANDSTOP FILTER DESIGN.....	40
5.3 DEVELOPMENT OF FREQUENCY SELECTIVE MULTIPLEXER LIMITER .....	41
<b>REFERENCES .....</b>	<b>49</b>

## FIGURES

1. N-channel channelizer. ....	6
2. First order cochlea channelizer. ....	7
3. Channelized RF receiver with tunable notch filters. ....	8
4. Cochlea mechanical to electrical transform. ....	9
5. Finite quality factor second order notch filter. ....	10
6. Basic design of absorptive notch various alternative architectures. ....	10
7. Basic design of absorptive notch various alternative architectures. ....	11
8. Frequency response of absorptive notch from Figure 7 varying the quality factor of the resonators.....	12
9. Proposed alternative lumped element absorptive notch filter.....	12
10. Frequency response of proposed absorptive notch filter. ....	13
11. Notional integration of channelizer with tunable notch filters. ....	14
12. Notional frequency response of RF channelizer + frequency agile notch filter. ....	14



13. Realization of tubular filter using transmission lines and surface mount capacitors. ....	16
14. Realization of each tubular channel filter. ....	16
15. Realization three-channel channelizer. ....	17
16. Fabricated prototype of three-channel channelizer. ....	17
17. Measured and simulated results. ....	18
18. Designed five-channel channelizer with capacitors in manifold. ....	19
19. Fabricated five-channel channelizer with capacitors in manifold. ....	19
20. Measured and simulated five-channel channelizer with capacitors in manifold. ....	20
21. C-Band five-channel cochlea channelizer. ....	21
22. Transmission line equivalent of tubular filter topology. ....	22
23. Input impedance of channel 1 prototype filter. ....	22
24. Schematic simulation in Keysight ADS. ....	22
25. Fabricated prototype 5-channel C-band channelizer. ....	23
26. Measured and simulated transmission coefficient. ....	24
27. Measured and simulated reflection coefficient. ....	24
28. Proposed fully tunable reflectionless bandstop filter. ....	25
29. Fabricated fully tunable reflectionless bandstop filter. ....	26
30. Simulated S21 and S11 of reflective and reflectionless designs. ....	27
31. S11 at 4.9 GHz sweeping R. ....	28
32. Measured S21 and S11 with varactor diode biased from 0–10 V. ....	<b>Error! Bookmark not defined.</b>
33. Measured 3-dB FBW, Resonant Frequency, and Bias Voltage. ....	29
34. Proposed reflectionless bandstop filter. ....	30
35. Contour plot of S21 and S11 when R1 and R2 are swept. ....	31
36. Fabricated fixed frequency prototype and TRL calibration substrate. ....	32
37. Measured and simulated S11 and S21. ....	33
38. Measured S21 phase. ....	33
39. Fabricated frequency tunable prototype and calibration substrate. ....	34
40. Measured frequency response of tunable prototype. ....	34
41. Prototype CLIC-SKIN for C-Band. ....	35
42. Prototype CLIC-SKIN for C-Band. ....	36
43. Printed Circuit Board Fabrication for absorptive bandstop filters, RF Channelizers, and CLIC-SKIN. ....	36
44. Printed Circuit Board Fabrication absorptive bandstop filters, RF Channelizers, and CLIC-SKIN. ....	37
45. Channelizer with embedded tunable notch filters. ....	39
46. X-band 5 contiguous channel frequency multiplexer. Designed on 10 mil fused silica. ....	40
47. Fabricated prototype of absorptive tunable bandstop filter for channel 2. ....	41
48. Measurement result of ABSF for channel 2. ....	41
49. Prototype of X-band frequency selective limiter using absorptive tunable notch filters embedded multiplexers. Prototype is 2.7 inches by 2.7 inches. ....	42
50. Channel characteristics of channel one with tunable notch filter (red line indicates 3dB). ....	43

51. Test use case setup for co-channel narrowband interferer. ....	43
52. Measurement results before (left) and after (right) ABSF is tuned to blocking signal. ....	44
53. Full frequency response of the five-channel channelizer with embedded absorptive tunable notch filters. ....	44
54. Test case for wide open RF front end for far out jammer. ....	45
55. Response of the receiver before and after a far out jammer is presented. ....	46
56. Test case for wide open RF Front End Close in Jammer. ....	46
57. Response of the receiver before and after a close in jammer is presented. ....	47
58. Test case for channelized RF front end. ....	47
59. Response of the receiver with channelization. ....	48

## TABLES

1. Required component values for topology shown in Figure 7 given 50 $\Omega$ system impedance at 2 GHz operating frequency. ....	12
2. Measured channelizer specifications. ....	25
3. Comparison between some published works on microwave notch filters. ....	38

# 1. PROJECT SUMMARY

The Navy is interested in anti-jam capabilities for bent-pipe satellite communication (SATCOM) systems. Legacy systems that receive substantial use include the Commercial Wideband Satellite Program (CWSP), which has link allocations in the C-band uplink (3.7–4.2 GHz) and downlink (5.85–6.42 GHz), Defense Satellite Communication System (DSCS), and Wideband Global SATCOM (WGS), which both have link allocations in the X/Ku-bands uplink (7.9–8.4 GHz) and downlink (7.25–7.75 GHz). All of these systems provide essential coverage to the warfighter on land, ocean, and air; however, these bent-pipe satellite communications (SATCOM) links are susceptible to jamming by an interferer, leading to denial of service. These systems have built-in interference mitigation techniques that include: frequency multiplexing, the use of guard bands to control emissions, and frequency hopping.

Wideband SATCOM systems are desirable to support high throughput links but are particularly susceptible to jamming by an interferer. For example, wideband radio-frequency (RF) front ends often employ a broadband low-noise amplifier (LNA). If the LNA receives a strong signal that is not the signal of interest (SOI) it can cause the amplifier to go into compression and become saturated. For wideband systems this becomes especially serious because the likelihood of spurious signals increases. One method to mitigate this effect is to frequency multiplex the bandwidth of interest, essentially channelizing the spectrum. Although frequency multiplexing the full spectrum into subchannels localizes failure to a subchannel, loss of a subchannel can still have tremendous repercussions, depending on the subchannel bandwidth. Therefore, the ability to mitigate interferer signals is essential.

To address the Navy's anti-jam interests, this report details a two-year Office of Naval Research (ONR) study as a Discovery and Innovation effort on this topic.

# 2. OVERVIEW OF TECHNICAL APPROACH

In response to interference cancellation, tunable high-quality (Q) band-pass/band-reject filtering technologies, and electronic protection techniques for bent-pipe SATCOM, this document aims to develop an RF/microwave comb limiter combiner channelizer with built-in tunable notch filter(s) for sub-band known interference cancellation. This development will enable interference-robust bent-pipe SATCOM systems. This is illustrated in Figure 1.

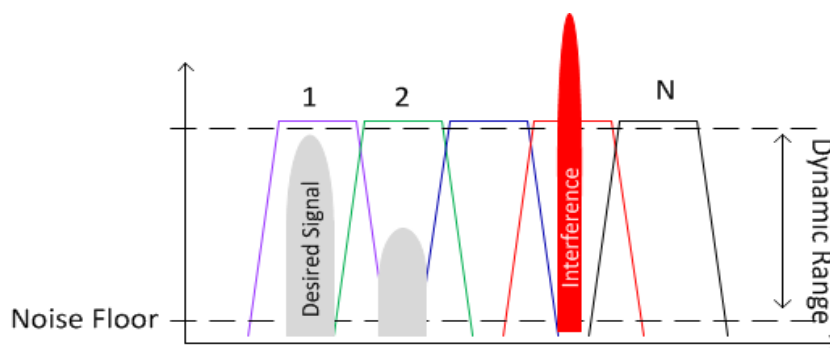


Figure 1. N-channel channelizer.

To allow for full dynamic range within a wideband spectrum, various levels of channelization are necessary. Software-defined radios use this technique, channelizing in the RF, intermediate frequency (IF), and digital domain [1]. The topic of frequency multiplexing has been investigated by the Naval Research Lab (NRL) [2], and various permutations of this architecture have reappeared over the years, including cryogenic channelizers [3]. Recently, the University of California San Diego (UCSD) has investigated channelizers modeled after the human cochlea, which demonstrate tremendous promise [4]. These cochlea-modeled channelizers achieve constant fractional bandwidth and can be realized using surface mount technology (SMT) or distributed transmission line techniques. This approach is favored and is the proposed architecture for this study. A first order cochlea channelizer is shown in Figure 2. This will be the first thrust area in our architecture study for the development of an efficient RF/analog channelizer.

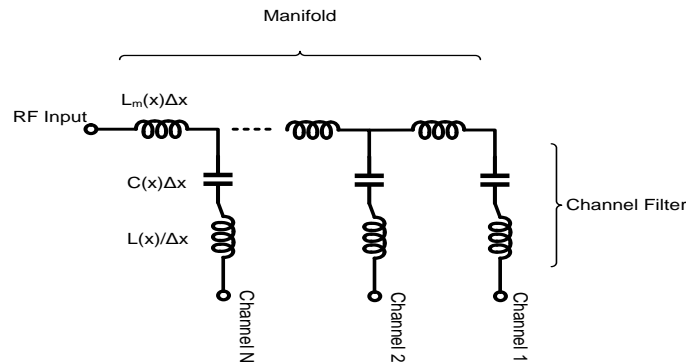


Figure 2. First order cochlea channelizer.

The second thrust area in our architecture is the development and integration of a highly tunable notch filter that exhibits characteristics of high spectral isolation. In recent years, much research has been performed in a new class of notch filters known as “absorptive notch filters.” Absorptive notch filters were first proposed in reference [5] and variations of this architecture are presented in [6–12], with much of the work performed by researchers at the NRL. This type of notch filter exhibits deep bandstop characteristics, which is typical of high-quality factor resonators. The absorptive notch filters are integrated with low-to-moderate quality factor resonators that are more realizable using non-exotic technologies. The ability to null or cancel continuous wave (CW) interference signals, which are high in power, is critical to the protection of the RF front end. We propose the integration of a frequency-agile and compact-tunable absorptive notch filter that is embedded into an RF channelizer to mitigate strong interferers, as shown in Figure 3. We notionally started in the C-band (4–8 GHz) and move into the X-band (7–11GHz) in the second year. The pursued thrusts can be summarized as:

- Development of an N-channel RF cochlea-based channelizer
- Development of a frequency-agile absorptive notch filter
- Integration of channelizer with tunable notch filter
- Interference-sensing mechanism

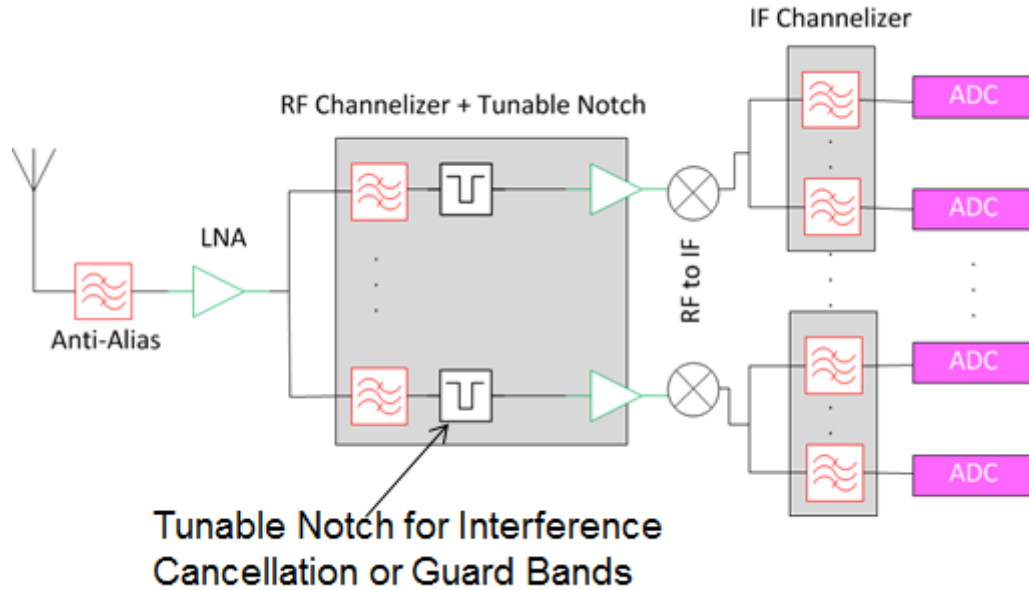


Figure 3. Channelized RF receiver with tunable notch filters.

## 2.1 BROADER IMPACT

The proposed research is of interest to the U.S. Navy specifically for bent-pipe SATCOM systems where interference mitigation is necessary. The RF architectures investigated are frequency and bandwidth adaptable, and therefore insights gained from this research effort may be valuable to other communities such as radar, communications, and information operations.

## 2.2 OUTLOOK OF THE NEW CAPABILITIES

The new capabilities developed in this project will enable wideband receivers to be more robust against potential interference, which can be self-generated or foreign in origin. This added level of protection from receiver compression will reduce the possibility of denial of service due to jamming.

# 3. PROJECT DESCRIPTION

## 3.1 COCHLEA-BASED RF CHANNELIZER DESIGN

Various architectures have been proposed in the design of microwave/RF channelizers. Efficient design methodologies have been proposed in reference [13] and the topic of cryogenic channelizers with low insertion losses have been demonstrated in reference [14]. While these approaches are sufficient, a more intuitive and succinct approach is proposed in reference [4], in which the channelizer is modelled after the human cochlea. In this approach, the basilar membrane acts as a dispersive transmission line for acoustic waves with a spatially dependent cutoff frequency. In a similar manner, an electrical/analog equivalent circuit can be derived that operates as a low-pass transmission line structure shunt loaded by series resonator sections. A 20-channel, 20–90 MHz constant fractional bandwidth channelizer is demonstrated in reference [4], a 10-channel 200–1022 MHz third order channelizer is demonstrated in reference [15], a 26-channel, 20–90 MHz channelizer is demonstrated in reference [16], and finally a 7-channel millimeter-wave (70–220 GHz) channelizer is demonstrated in reference [17], all utilizing the cochlear model. Figure 4 shows the mechanical to electrical transform of the cochlear model. We plan on developing either lumped element circuit or

distributed transmission line models of the channelizer in the C-band. For X-band, we anticipate using transmission line equivalent circuits to reduce loss and parasitics. We plan on exploring the trade-space to determine the number of channels that can be accommodated while still being able to realize the circuit. For the C-band, we plan to cover from 3–6 GHz, and in the X-band we plan to cover from 7–10 GHz.

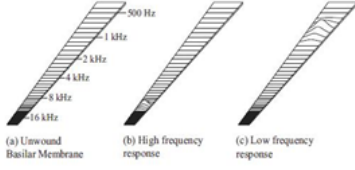
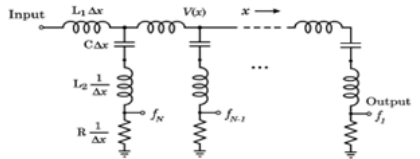
	Mechanical	Conversion	Electrical
Technology	 <p>(a) Unwound Basilar Membrane (b) High frequency response (c) Low frequency response</p>	<p><math>x</math> – position along the structure  <math>P(x)</math> – fluid pressure <math>\leftrightarrow V(x)</math>  <math>H</math> – duct height  <math>\rho</math> – fluid density  <math>\frac{\rho}{H} \leftrightarrow L_1(x)</math>  <math>k(x)</math> – stiffness <math>\leftrightarrow \frac{1}{C(x)}</math>  <math>m(x)</math> – mass <math>\leftrightarrow L_2(x)</math>  <math>r(x)</math> – damping <math>\leftrightarrow R(x)</math></p>	
System Design	$\frac{d^2 P(x)}{dx^2} + \frac{\rho}{1 + j\omega \frac{r(x)}{k(x)} - \omega^2 \frac{m(x)}{k(x)}} \omega^2 P(x) = 0$		$\frac{d^2 V(x)}{dx^2} + \frac{L_1(x)C(x)}{1 + j\omega R(x)C(x) - \omega^2 L_2(x)C(x)} \omega^2 V(x) = 0$

Figure 4. Cochlea mechanical to electrical transform.

### 3.2 EQUENCY AGILE ABSORPTIVE NOTCH FILTERS

Channelizers allow the ability to sub-divide a wide spectrum into smaller sub-bands, and this partially solves the challenge of preserving the dynamic range when a strong interferer is present. However, even while channelizing, a strong interferer's presence can cause an entire sub-band to be saturated and effectively wiped out. This can be detrimental to communication systems and can cause links to be error prone or completely lost. The ability to mitigate a known interferer within a sub-band is therefore critical. One method of achieving this is through the use of a tunable notch filter that can tune across the entire frequency multiplexed spectrum. The ability to effectively reject the interferer's signal within the sub-band relies greatly on the achievable notch depth, which is often related to the quality factor of the notched resonator. For example, Figure 5 shows a conventional second order notch filter with a finite  $Q$ . The depth of the notch improves with increasing quality factor. However, the quality factor that one can realize is greatly limited in reality by how the resonator is physically realized. For example, using monolithic processes, the quality factor of a resonator can range from 4–25 [18]. On multi-chip module (MCM) technology like low temperature co-fired ceramic (LTCC) or liquid crystal polymer (LCP), the achievable  $Q$  is on the order of 25–150 [19]. Using exotic technologies such as microelectromechanical-systems (MEMs), surface acoustic waves (SAW), or bulk acoustic waves (BAW) devices, one can achieve  $Q$  on the order of 400+ [20]. Although improving the quality factors of resonators is important, there is certainly a technological limit in terms of their physical realization, thus notch filter architectures that are not dependent on the quality factor become important.

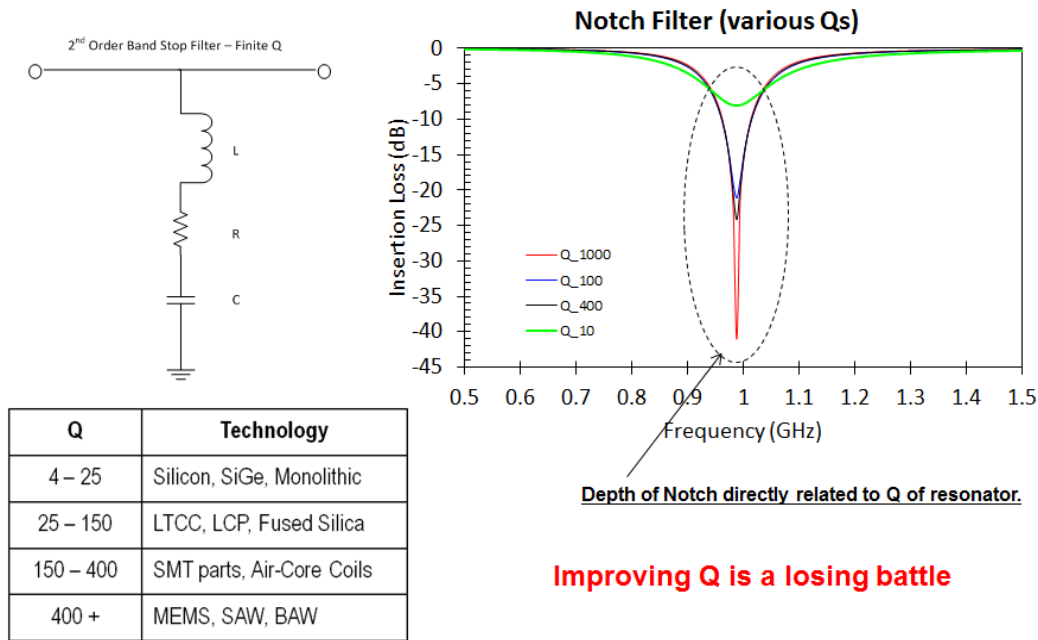


Figure 5. Finite quality factor second order notch filter.

Recently, Jachowski (NRL) has proposed a notch filter architecture that is independent of the quality factor of the resonators [5], instead relying on phase cancellation. This type of filter is also unique in that it is impedance matched outside its stopband. This method has been termed as an absorptive notch filter and has been realized in various permutations. The most basic design is shown in Figure 6 and is comprised of an all pass filter with a  $90^\circ$  delay, which is parallel with a second order bandpass filter (BPF). The second order BPF has a phase response of  $-90^\circ$  at resonance; therefore, the two paths are  $180^\circ$  out of phase exactly at the resonant frequency. This means the two transfer functions are subtractive and form a notch transfer function. The notch is therefore dependent on the precision of the phase subtraction rather than the quality factor of the resonators. The notch filter is also well matched out of band as well as in-band. Variations of this “absorptive” notch filter have been proposed and demonstrated in literature, and some are designed to be tunable. Figure 7 shows a simple absorptive notch that utilizes mutual coupled inductors. This approach, proposed by Purdue University is preferable due to its simpler realization [12].

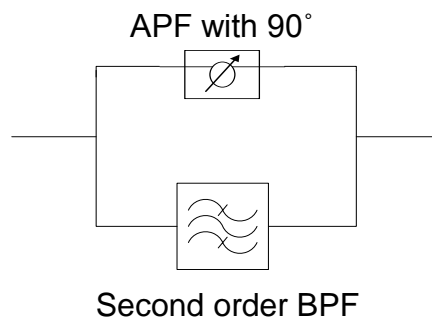


Figure 6. Basic design of absorptive notch various alternative architectures.

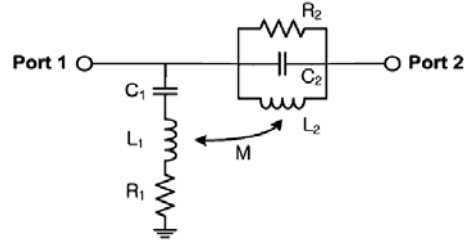


Figure 7. Basic design of absorptive notch various alternative architectures.

Although the absorptive filter architecture alleviates the need for high quality factor resonators to achieve high rejection, the bandwidth of the filter is still correlated with the quality factor of the resonator. Equation 1 shows this relationship, where  $L_s$  is defined as the stopband edge attenuation value.

$$BW = 2 / \left( Q_u \sqrt{10^{L_s/10} - 1} \right) \quad (1)$$

The design in Figure 7 shows that as the quality factor of the resonators increases, the bandwidth of the notch filter decreases, making sharper response. Figure 8 illustrates this behavior. It is important to note that widening the bandwidth of these notch filters is straightforward because multiple absorptive notch filters can be cascaded to gain that effect. However, narrow bandwidth notch filters are more difficult to develop, as high-quality factor resonators are necessary. Narrow bandwidth notch filters are more desirable for this application because as the number of channels increases within a channelizer, the sub-bands become narrower as they approach the stopband edges of the notch filter. Although the approach in reference [12] is elegant and requires minimal components, the architecture requires a unique solution. For a given system impedance, quality factor, and center frequency, there is only one set of component values that fulfill the requirements. As such, this design is difficult to realize over wide operating requirements. For example, Table 1 shows some of the required inductor values given a system impedance of  $50\Omega$  at an operating frequency of 2 GHz. To achieve mid- to high-quality factors, high-value RF inductors are necessary, which cannot be developed. This topology certainly has its limitations.

We therefore propose to investigate alternative architectures that are highly miniaturized as demonstrated in reference [12] but with more degrees of design freedom. One proposed architecture is shown in Figure 9. This variation on Bode's original topology [21] allows for more design freedoms, which lead to a design easier to develop.



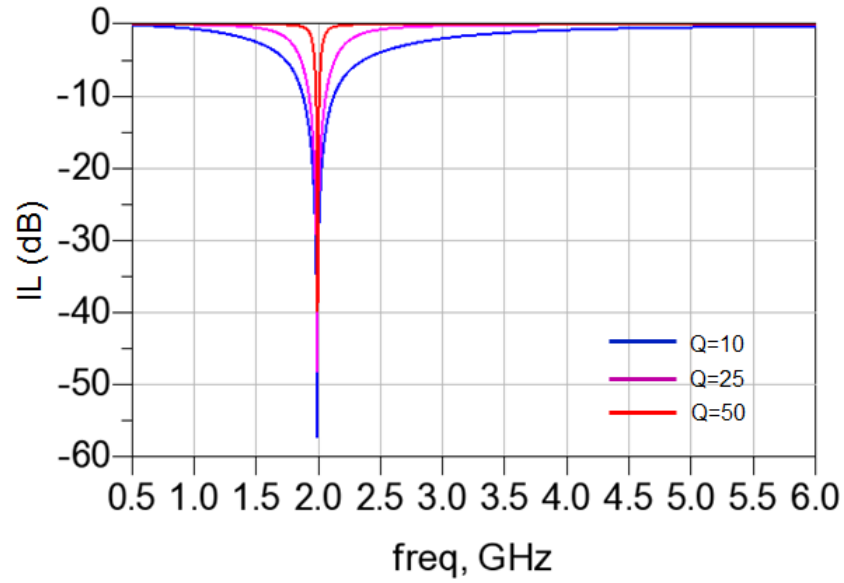
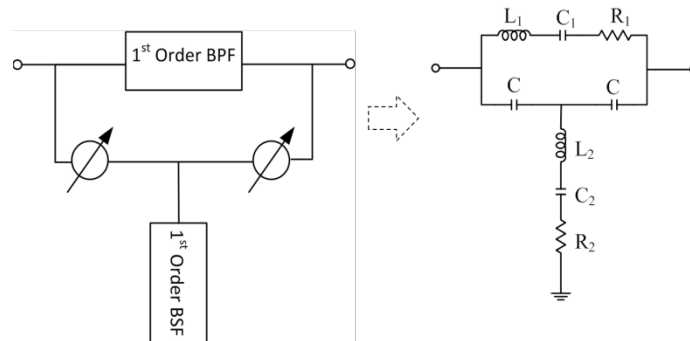


Figure 8. Frequency response of absorptive notch from Figure 7 varying the quality factor of the resonators.

Table 1. Required component values for topology shown in Figure 7 given 50Ω system impedance at 2 GHz operating frequency.

Q	$L_1$ (nH)	$C_1$ (pF)	$R_1$ (Ω)	$L_2$ (nH)	$C_2$ (pF)	$R_2$ (Ω)	M(nH)
10	20	3.1	25	0.79	7.95	100	0.39
25	49.7	0.13	25	0.32	19.9	100	0.16
50	99.4	0.06	25	0.16	39.7	100	0.07



Q	$L_1$ (nH)	$C_1$ (pF)	$R_1$ (Ω)	$L_2$ (nH)	$C_2$ (pF)	$R_2$ (Ω)	C (pF)
20	15	0.49	15	15	0.41	24	4.6

Figure 9. Proposed alternative lumped element absorptive notch filter.

As an example, given a system impedance of  $50\Omega$ , an operating frequency of 2 GHz, and a quality factor of 20, the required inductance is only 15 nH, which is within the bounds of lumped element realization. Figure 10 shows the frequency response of this notch filter in comparison with the design proposed in reference [12]. The only drawback of the proposed design is that it requires 4 inductors.

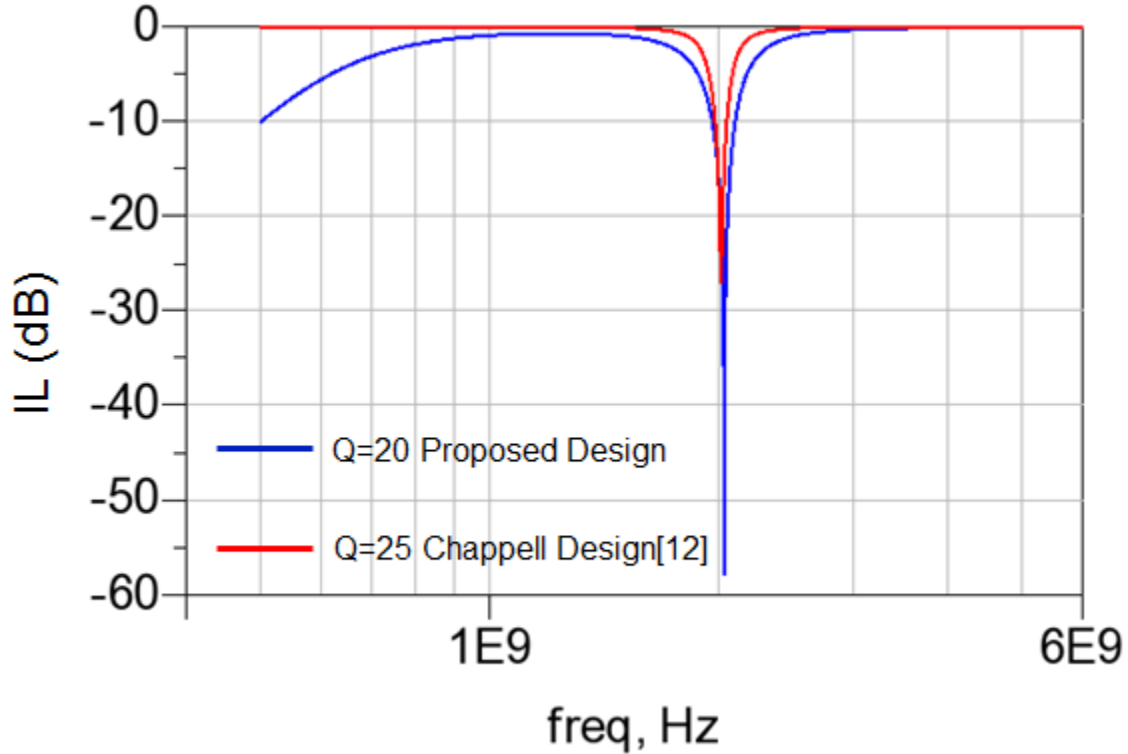


Figure 10. Frequency response of proposed absorptive notch filter.

### 3.3 INTEGRATION OF CHANNELIZER WITH FREQUENCY AGILE NOTCH FILTER

To mitigate an interfering signal within a channelizer sub-band, we propose a study of various channelizer + absorptive notch architectures. A notional design is shown in Figure 11 where tunable notch elements are embedded within each sub-band, as well as a tunable notch preceding the channelizer to create a guard band. Figure 12 shows simulated results using a single absorptive notch, and the simulation suggests greater than 50 dB rejection can be achieved from reactive components that have easily achievable quality factors. The notch can be made digitally tunable by adding varactors, which are controlled by digital to analog converters (DACs). The order of both the channelizer and absorptive notch can be adjusted to be application specific. For example, a third order cochlea channelizer can be designed if greater stop band attenuation is required.

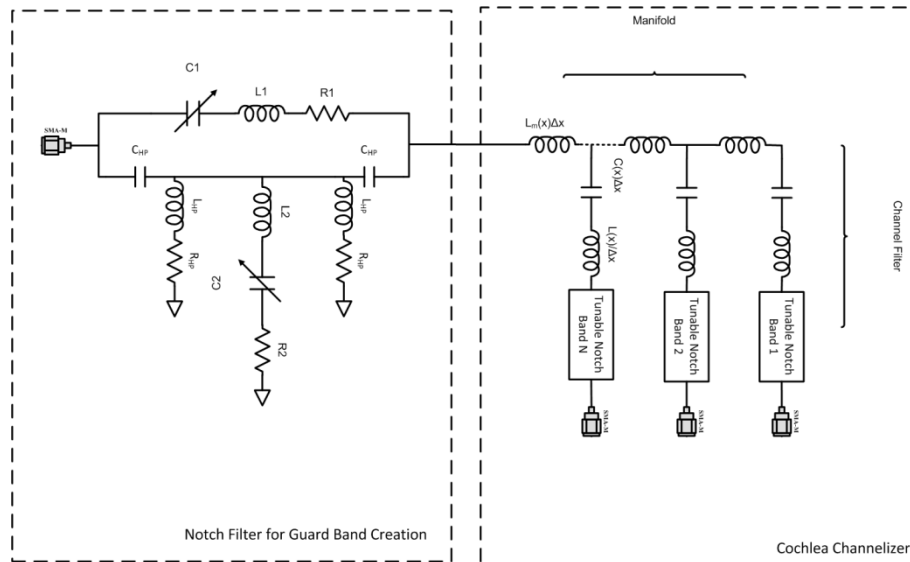


Figure 11. Notional integration of channelizer with tunable notch filters.

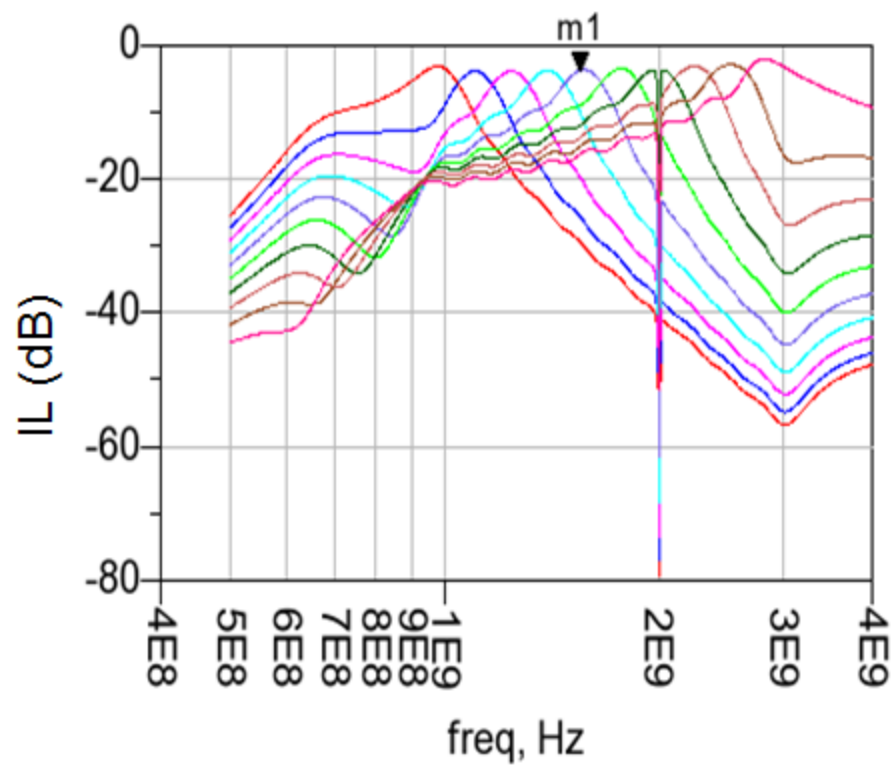


Figure 12. Notional frequency response of RF channelizer + frequency agile notch filter.

## 4. TECHNOLOGY DEVELOPMENT IN C-BAND

The objective of the first year of the study was to develop an RF channelizer with a built-in tunable notch filter that is capable of supporting bent-pipe SATCOM systems, notionally in the C-Band. This project will follow the aforementioned project description and corresponding technical approaches.

### 4.1 DEVELOPMENT OF COCHLEA CHANNELIZER

#### 4.1.1 Three-Channel Design Using Lumped Capacitors

In our first iteration of the cochlea-based channelizer design, we opted the use of tubular filters to realize each channel filter. In reference [15] and reference [16], we used this method to develop channelizers in the MHz frequency regime where lumped elements were used. However, in the C-Band, lumped element use is limited to only capacitors as the self-resonant frequencies (SRF) for surface mount inductors are typically below frequencies in the C-Band. For this reason, transmission line equivalent models are utilized, such as in reference [17].

To gain an understanding on design limitations for this type of microwave channelizer, a simple three-channel channelizer was designed as a starting point. As in reference [17], transmission lines were used to realize an equivalent circuit to the tubular filter architecture. This is shown in Figure 13. In this first iteration design, series inductors and shunt capacitors were realized using transmission lines. High impedance meandered lines create series inductors. Wide low impedance lines provide the parallel plate capacitance to ground, which create the shunt capacitors. Series capacitors are realized using AVX<sup>®</sup> surface mount capacitors. These AVX<sup>®</sup> capacitors are modelled in Keysight<sup>®</sup> ADS using libraries from Modelithics<sup>®</sup>. Each tubular channel filter was designed so that at its resonant frequency the filter was matched to 50 $\Omega$ , and for all frequencies below and above the resonant frequency the filter looked like an open circuit. This is illustrated in Figure 14. Once the channel filters are designed, each of the filters are coupled together through the manifold. In reference [15] and reference [16], the manifold is realized using inductors or high impedance lines. For low frequency designs this isn't a problem, but at high frequencies this can impose practical challenges by routing the fan-out for each of the channels because high impedance lines are often short and narrow transmission lines, whereas long transmission lines are desired to enable fan-out routing.

To overcome this practical challenge, series capacitors were inserted along the manifold feed to compensate and resonate out the extra length of transmission line that was inserted to allow for routing. This is shown in Figure 15. This design is on 40-mil Rogers 4350B substrate ( $\epsilon_r=3.66$ ,  $\delta=0.004$ ). Fabrication of this prototype channelizer/triplexer was done at Space and Naval Warfare Systems Center Pacific (SSC Pacific) and is shown in Figure 16. Full wave simulations of the channelizer were completed in both Agilent<sup>®</sup> Momentum and Ansys<sup>®</sup> HFSS. The measured and simulated responses for the prototype are shown in Figure 17. The channelizer operates from 2–8 GHz, with each channel having a 3-dB bandwidth of over 1.58 GHz.

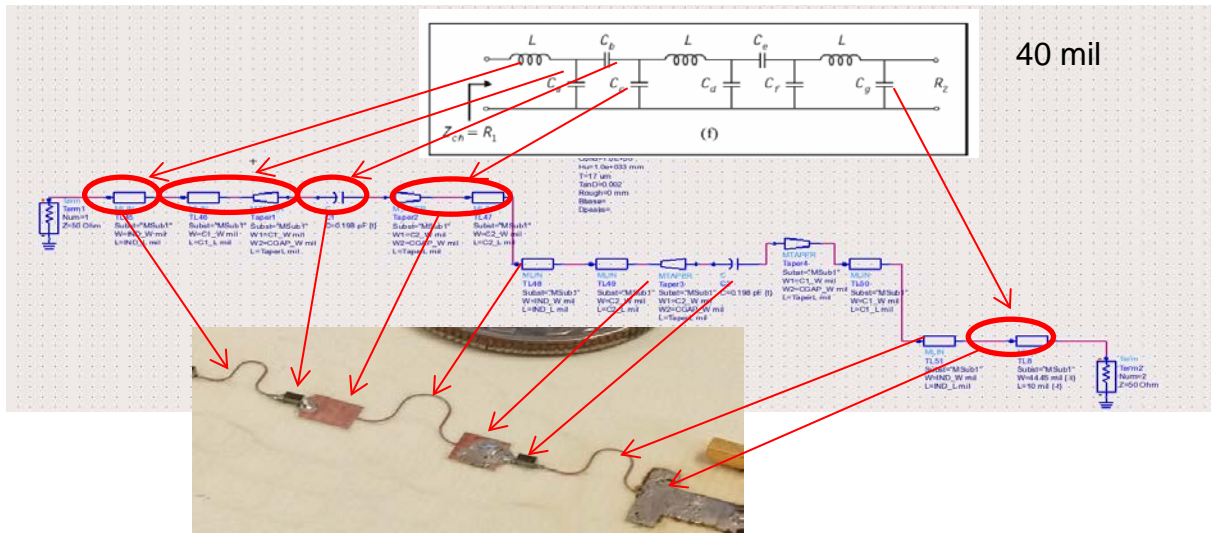


Figure 13. Realization of tubular filter using transmission lines and surface mount capacitors.

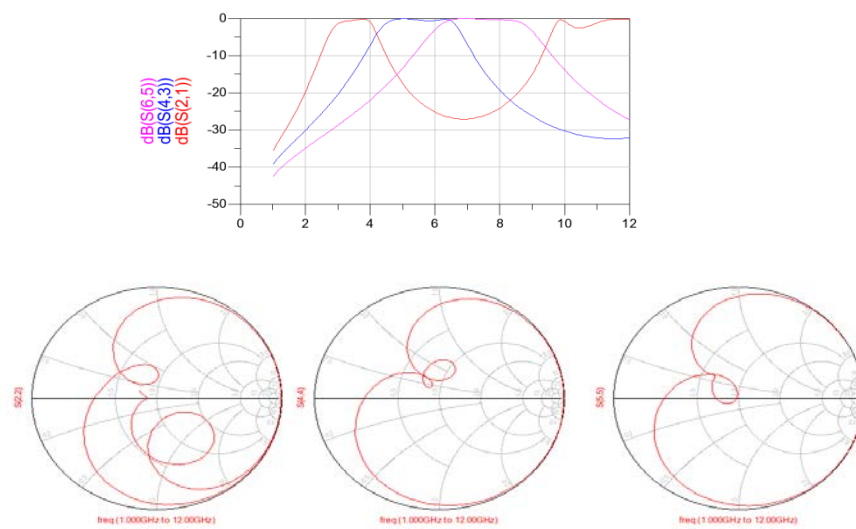


Figure 14. Realization of each tubular channel filter.

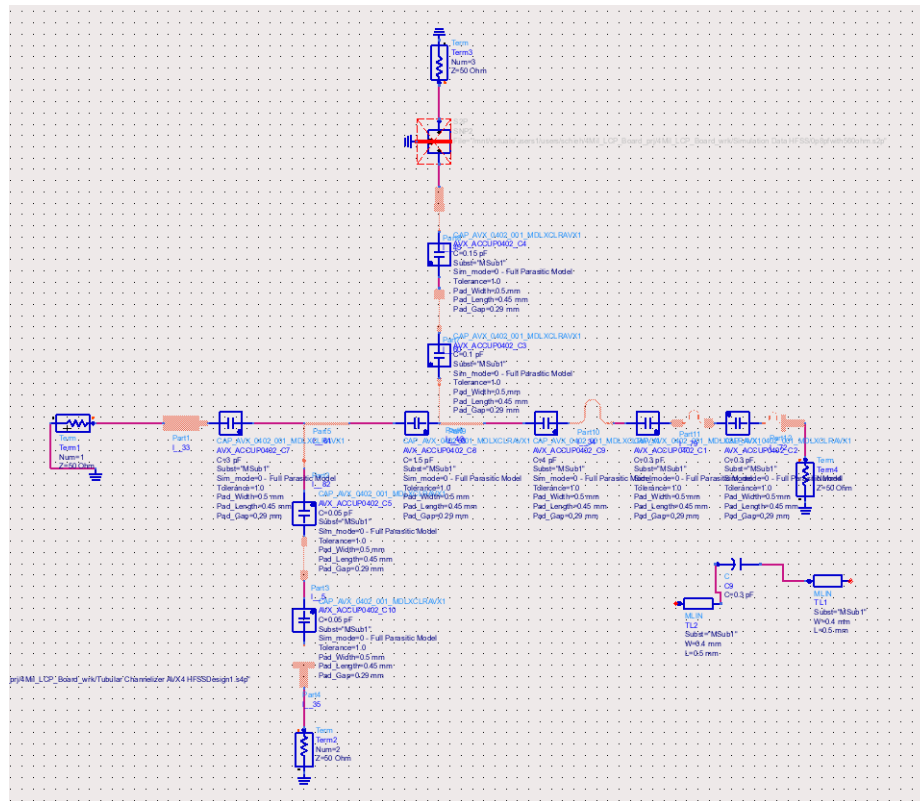


Figure 15. Realization three-channel channelizer.

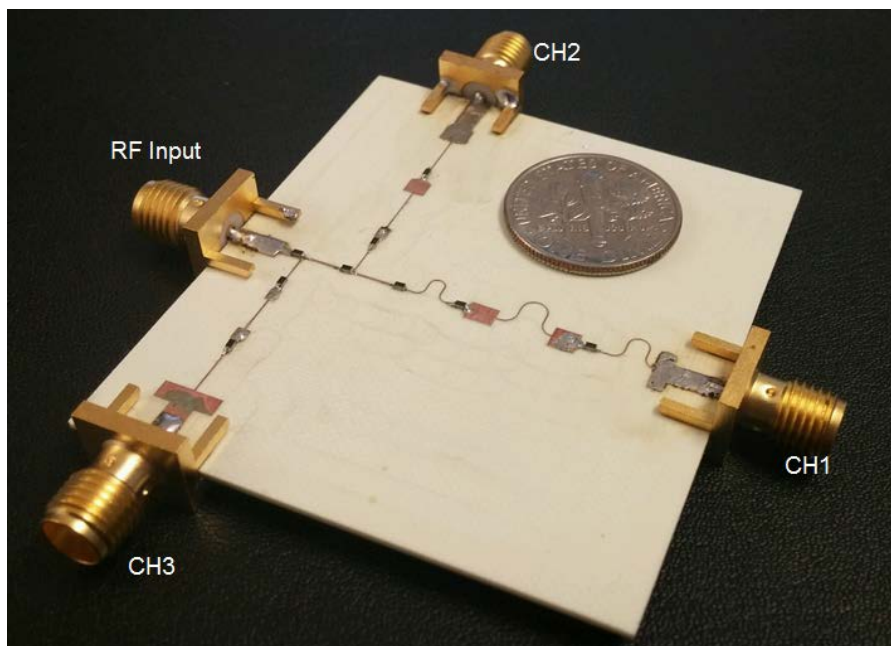


Figure 16. Fabricated prototype of three-channel channelizer.

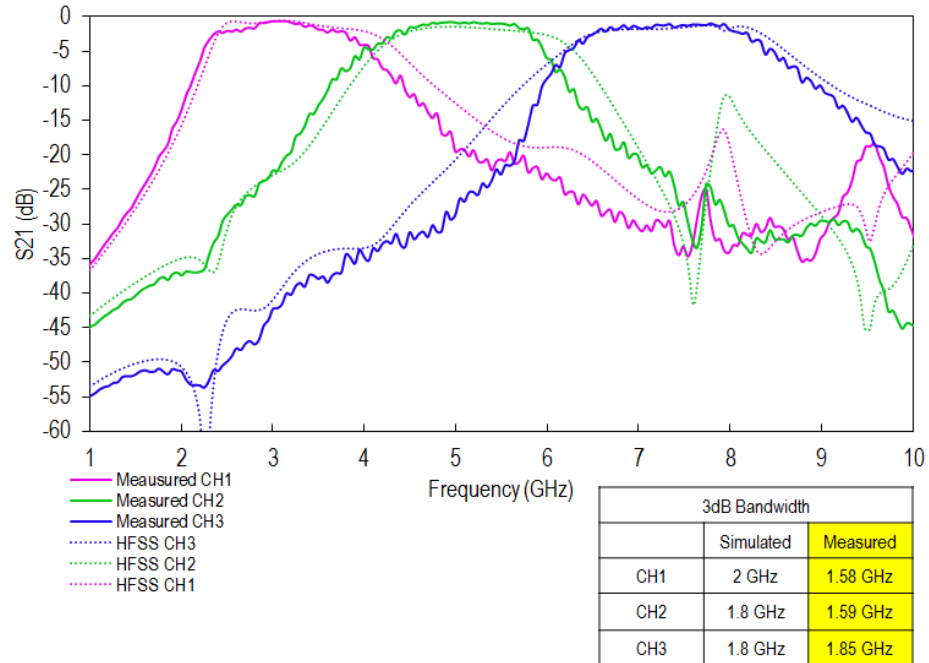


Figure 17. Measured and simulated results.

#### 4.1.2 Five-Channel Design using Lumped Capacitors

A second iteration design was completed for a five-channel channelizer. Using the same technique, this channelizer operates from 3–11 GHz with channel bandwidths of greater than 1.1 GHz. In this design, we sought to reduce the number of surface mount components because the surface mount parts have the highest variation in terms of modeling. In this case, series capacitors in the tubular filter are replaced with edge coupled transmission lines, which is shown in Figure 18. The fabricated prototype is shown in Figure 19. This iteration of the design simplified the modelling; however, the bandwidths of each channel is still much too large and covers more than the C-band. The measured and simulated responses for the prototype are shown in Figure 20.

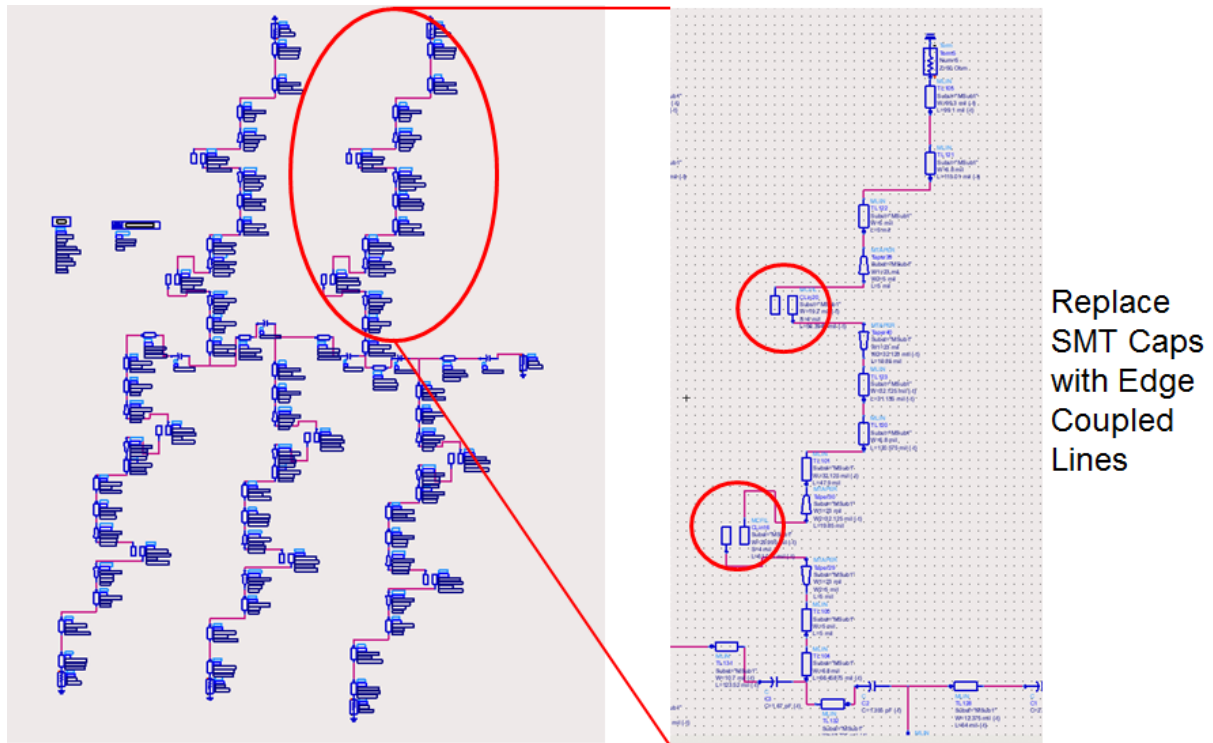


Figure 18. Designed five-channel channelizer with capacitors in manifold.

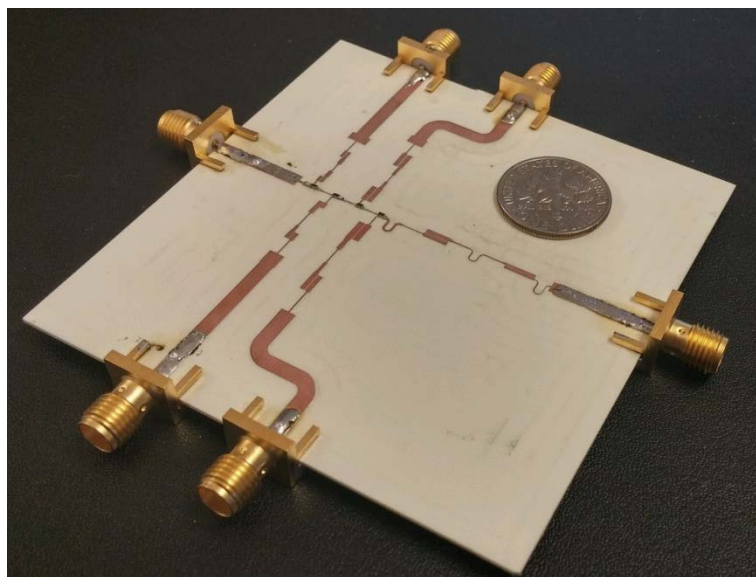


Figure 19. Fabricated five-channel channelizer with capacitors in manifold.



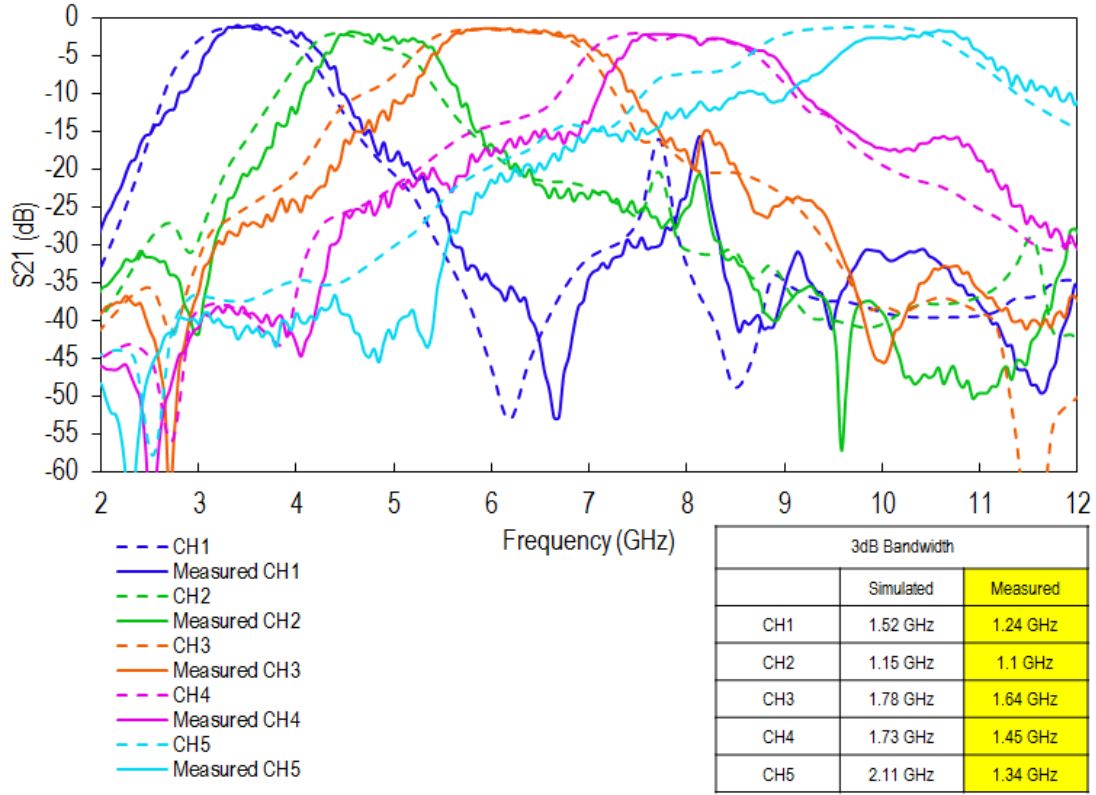


Figure 20. Measured and simulated five-channel channelizer with capacitors in manifold.

#### 4.1.3 Five-channel design for C-Band

As multi-functional RF systems become ubiquitous, the need increases for receivers to handle larger bandwidths. Although this is desirable, designing wideband receivers can be very challenging. Issues such as saturation and intermodulation distortion due to high power interferers can limit the allowable bandwidth a wideband receiver can accept. For this reason, channelizing filters can be especially desirable. Channelization splits the wide bandwidths into smaller portions, limiting detrimental effects to other channels when one channel is degraded while preserving high selectivity [22].

Various types of channelizer topologies have been proposed. One bio-inspired topology is based on the mammalian cochlea [23; 24], where the resonant frequencies of the parallel beams are organized from high to low frequencies. This method is also demonstrated in reference [16] and an inverse topology in reference [25]. All of the aforementioned designs were done at low frequencies below 1 GHz using lumped elements to realize each channel filter. At microwave frequencies, lumped element implementations simply are not viable. In reference [26] a microwave design is presented using a monolithic process; however, because lumped elements were used, the performance of the channelizer was severely degraded. In reference [27] a microwave design is presented; however, it requires a high temperature superconductor substrate. In reference [17] a W-band channelizer is presented using the cochlear approach. In this design, co-planar transmission lines were used to realize the tubular filters needed for the channelizer. This design was also fabricated using micro-fabrication processes.

This section presents the design of a cochlea-based RF channelizer operating in the C-band, which supports 5 contiguous channels. The design is realized at board level using transmission lines, and

covers frequencies from 3–8 GHz with channel bandwidths of no less than 0.74 GHz. The proposed channelizer is shown in Figure 21.

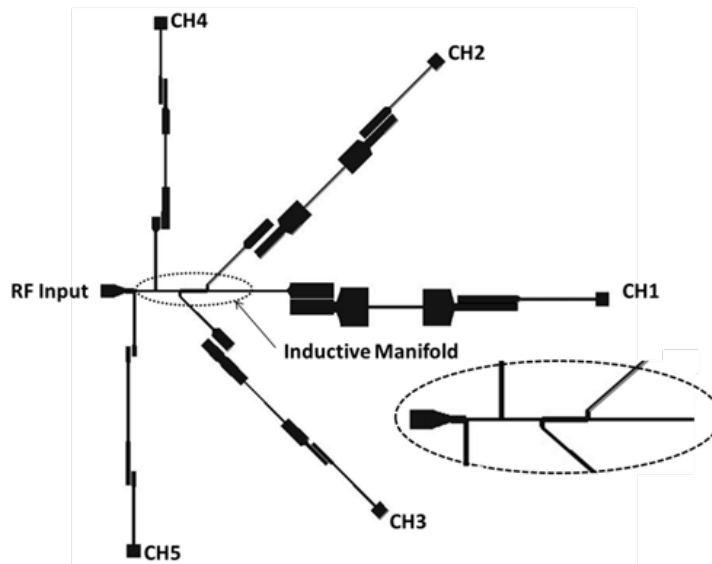


Figure 21. C-Band five-channel cochlea channelizer.

Critical to the operation of the cochlea-based channelizer is the impedance characteristic of each channel. Specifically, the input impedance of each of the channel filters should behave as a series resonator and appear as a short circuit at resonance and an open circuit at all other frequencies. The channels are coupled through an inductive manifold, which forms an up-converting ladder network transforming the channel impedance to the input impedance. As described in reference [24] and reference [16], there are not many filter topologies that satisfy the above requirements, with the exception of the tubular topology.

Typically, the tubular channel filters are realized using lumped elements. However, at microwave frequencies this is not possible because of low the self-resonant frequencies of surface mount inductors and capacitors. Instead, transmission line equivalent circuits are adopted as in reference [17]. Series inductors are realized as high impedance transmission lines. Series capacitors are realized using edge-coupled transmission lines. Shunt capacitors to ground are realized using wide transmission lines that have a parallel plate capacitance to ground. This is shown in Figure 22. Each channel filter is designed so that the input impedance resembles that of a series resonator. The input impedance of the BPF in channel one is shown in Figure 23. The filters are implemented in microstrip on a 40-mil thick Rogers® 4350B substrate ( $\epsilon_r = 3.66$ ,  $\delta = 0.0037$ ). Once each channel filter has been designed, they are aggregated and coupled via the manifold, which is comprised of high impedance inductive traces. The trace width of the high impedance lines are 6 mils. Once the filters are connected to the manifold, further channel filter optimization is necessary as distributed effects are prominent at microwave frequencies. Schematic level transmission line simulations were performed in Keysight® ADS [9] and are shown in Figure 24. The channelizer covers all of C-band and maintains a return loss of better than 10 dB. Each of the channel filters cover over 0.74 GHz of bandwidth. The adjacent band rejection can be improved by employing higher order channel filters; however, this is at the expense of incurring a higher insertion loss due to longer channel filters. Ansys® Designer is used to simulate the final transmission line design. The fabricated prototype is shown in Figure 25.

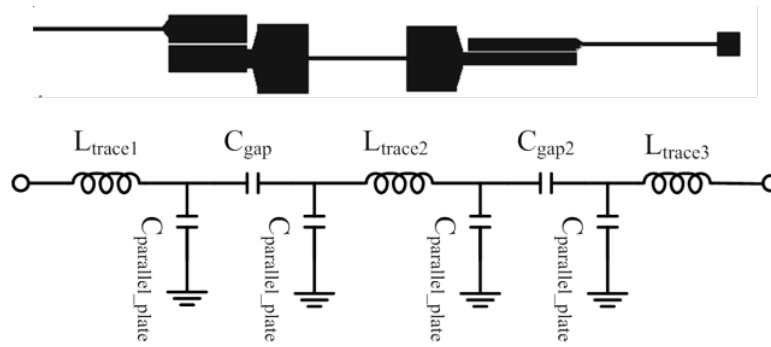


Figure 22. Transmission line equivalent of tubular filter topology.

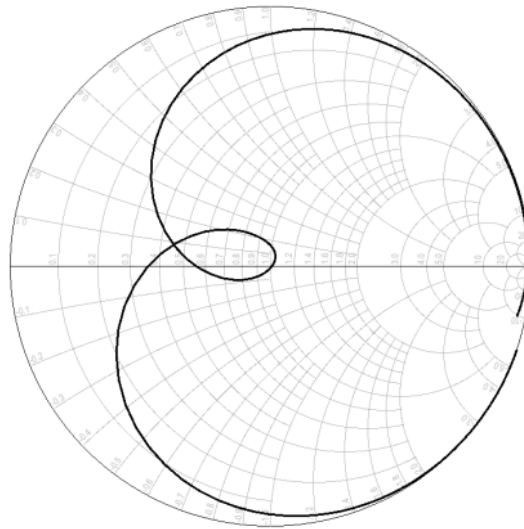


Figure 23. Input impedance of channel 1 prototype filter.

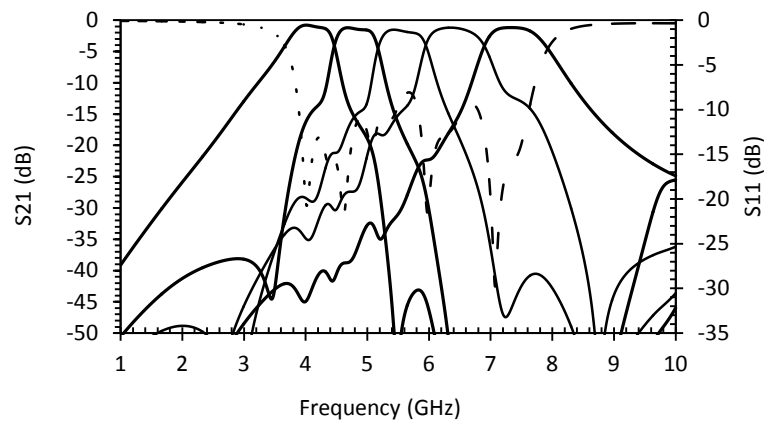


Figure 24. Schematic simulation in Keysight ADS.

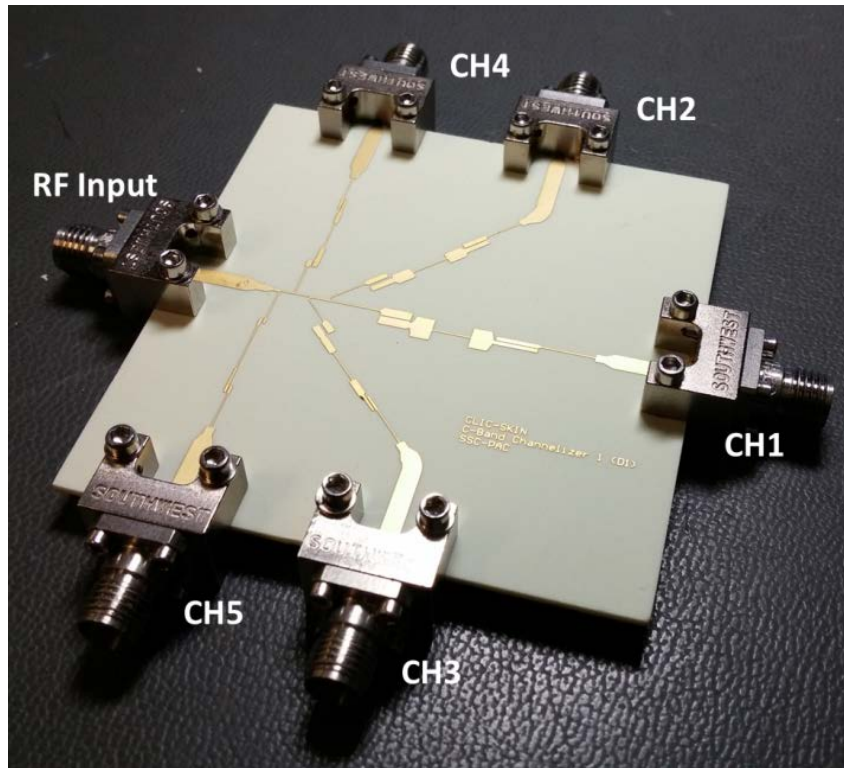


Figure 25. Fabricated prototype 5-channel C-band channelizer.

The channelizer's S-parameters are measured using an Agilent® N230C vector network analyzer. A custom thru-reflect-line (TRL) calibration kit was designed and used to de-embed both the coaxial fixtures used for the measurements, and 5.5 mm of  $50\Omega$  transmission line to reduce measurement loss. The input reflection coefficient is measured when all channel outputs are loaded with a  $50\Omega$  termination. The transmission response of a single channel is measured when all other channels are terminated with  $50\Omega$  loads.

The measured and simulated S-parameters for all five channels are shown in Figure 26 and Figure 27, respectively. A summary of the measured results are shown in Table 2. The channelizer maintains an S11 of better than -10 dB across the majority of the C-band, with exception to a slight mismatch at 4.86 GHz. The measured and simulated responses are fairly well correlated. The 3 dB bandwidth of each of the channel filters are each less than 1 GHz and can be further tuned to provide equal bandwidths. The measured insertion loss at the center frequencies of each channel filter does not exceed 2.26 dB. The crossover point between adjacent channels is around -6 dB. The adjacent channel rejection is measured from the center frequency to the upper and lower adjacent channels and is  $> 11$  dB.

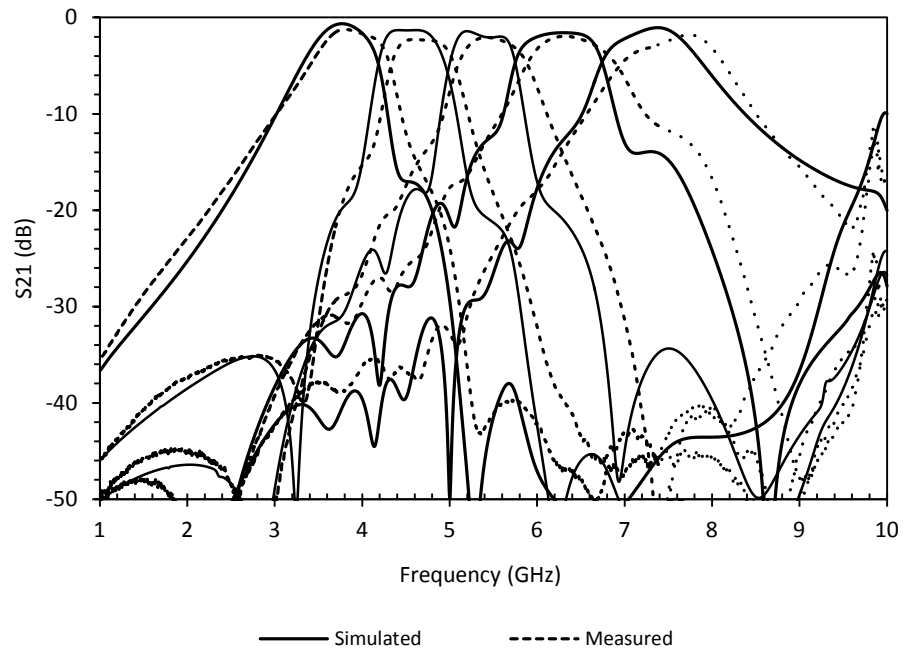


Figure 26. Measured and simulated transmission coefficient.

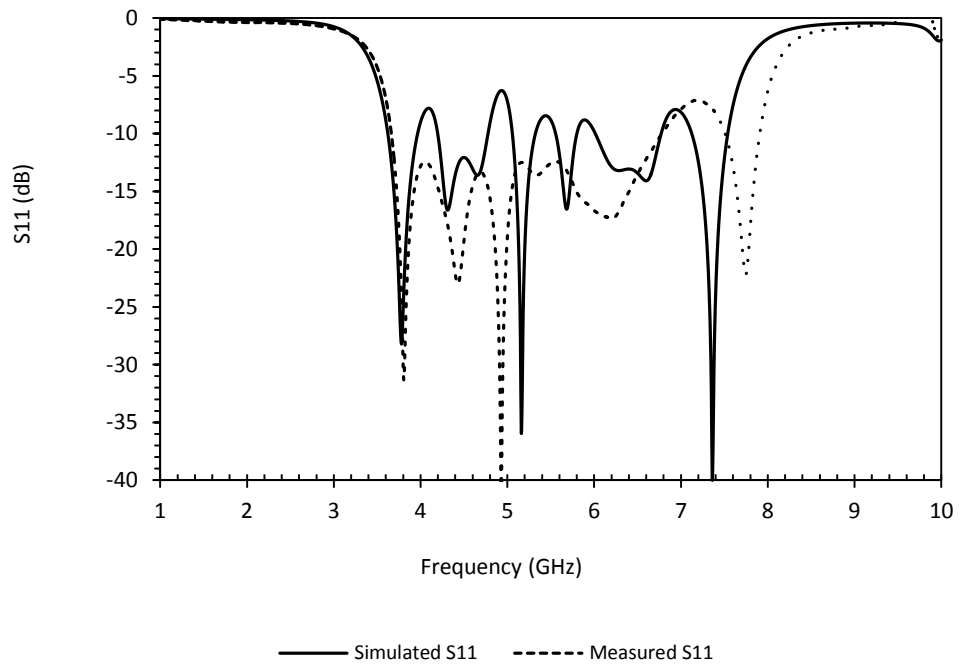


Figure 27. Measured and simulated reflection coefficient.

Table 2. Measured channelizer specifications.

Ch	Band-edge	$\Delta_3$ dB (GHz)	I.L.	Rejection N-1(dB)	Rejection N+1(dB)
1	3.45/4.29	0.84	1.23	-	17.16
2	4.32/5.06	0.74	2.26	16.32	14.25
3	5.08/5.89	0.81	2.06	17.9	11.72
4	5.88/6.90	1.02	1.92	16.11	12.53
5	6.92/8.13	1.21	1.79	11.84	-

## 4.2 ABSORPTIVE NOTCH FILTER DESIGN

### 4.2.1 Design based on coupled transmission lines

Modern microwave communication systems are often wideband by design. An example would be many recent software-defined radios that use very wideband RF front ends, which are especially susceptible to strong interferers. One mitigation technique is to use microwave channelizers. Another often-used technique is the ability to precisely excise the undesired signal through the use of tunable bandstop filters (BSF) [26]. Typical BSFs are reflection type, where the undesired signal is reflected back to the input and therefore rejected. However, recently there has been interest in reflectionless or “absorptive” BSFs where the undesired signal is absorbed rather than reflected, resulting in good input matching both in-band and out-of-band. In reference [28] and reference [29], an absorptive BSFs is realized on a transmission line using a phase cancellation approach. In reference [9], authors use lossy resonators to realize perfectly matched BSFs. Lumped element realizations are also proposed in references [11], [30], and [31] would enable further miniaturization. One interesting approach proposed in reference [32] improves on the traditional coupled transmission line BSFs with a small addition of a resistor at the input resonator to achieve the reflectionless characteristic. This approach is simple and convenient, as multiple sections can be cascaded to realize more rejection. Also, closed form design equations are available for this type of filter, which can be used to tune the performance. In this section, L-Resonators with open stubs [33] are adopted, which is in contrast to the short circuit coupled transmission lines presented in reference [32].

The proposed reflectionless BSFs shown in Figure 28, where a four-stage design is presented. The filter is composed of four resonator sections; however, only the first section (inside the dashed box) needs to be analyzed to understand the reflectionless properties.

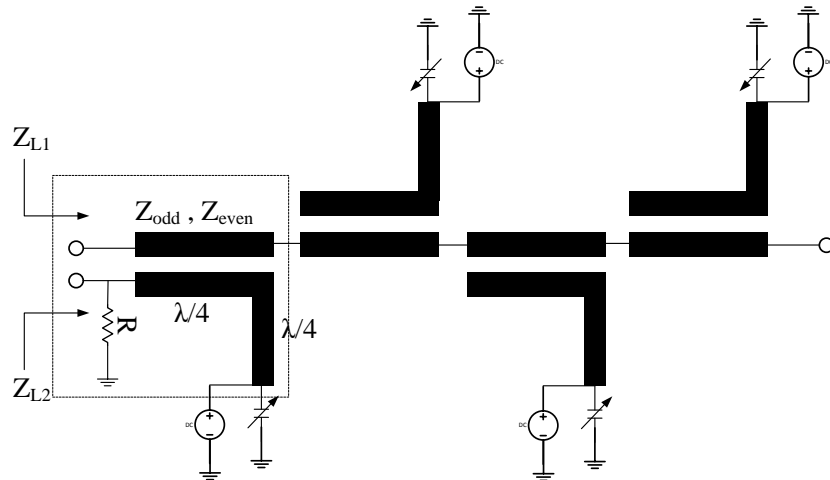


Figure 28. Proposed fully tunable reflectionless bandstop filter.

According to reference [34], the resonator behaves as a BPF where the image impedances of the first quarter wave resonator are defined as

$$Z_{L1} = \sqrt{Z_{odd}Z_{even}} \left( \frac{Z_{even} - Z_{odd}}{Z_{even} + Z_{odd}} \right) \quad (2)$$

$$Z_{L2} = \frac{Z_{even}Z_{odd}}{Z_{L1}} \quad (2). \quad (3)$$

When the input port is terminated by the characteristic impedance,  $Z_o$  (which is  $50\Omega$ ), the value of  $R$  can be readily solved such that it absorbs all the power, this is determined to be:

$$R = Z_o \left( \frac{Z_{even} + Z_{odd}}{Z_{even} - Z_{odd}} \right)^2. \quad (4)$$

The design of the bandstop response follows from [35] where a low pass prototype is first used and the normalized reactance slopes for each resonator section are determined as follows:

$$\frac{x_i}{Z_o} = \frac{g_o}{g_i \Omega_c FBW} \text{ for } i = 1 \text{ to } n, \quad (5)$$

where  $\Omega_c$  is the cutoff frequency, FBW is the fractional bandwidth, and  $g_i$  is typically determined from a look-up table. The prototype design is shown in Figure 29, fabricated on 40-mil Rogers® 4350B. For simplicity, all 4 coupled line sections are made to be equal with  $Z_{odd} = 46.4\Omega$  and  $Z_{even} = 75.75\Omega$ . From Equation 4, an  $866\Omega$  resistor would be optimal; however, in practice a 1- k $\Omega$  resistor was utilized because of general availability.

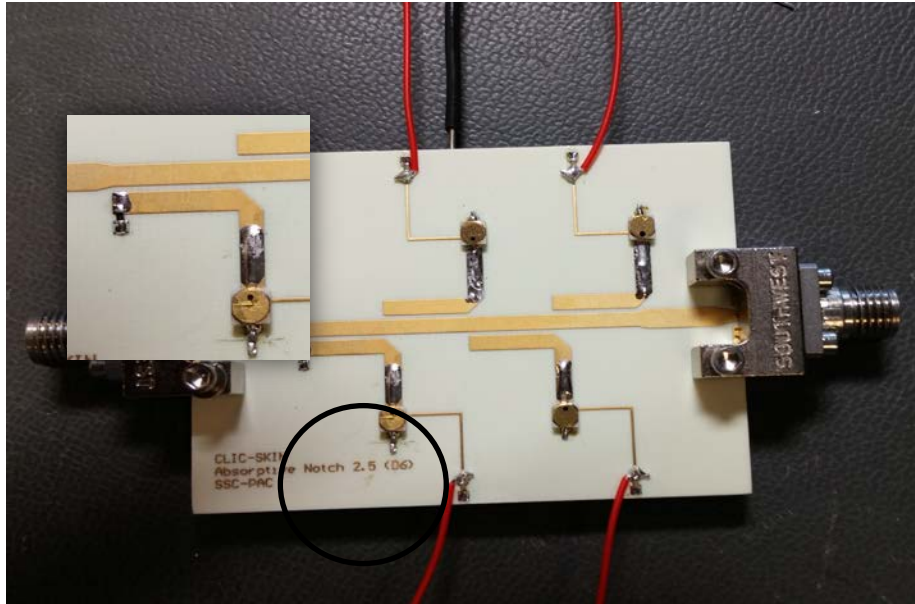


Figure 29. Fabricated fully tunable reflectionless bandstop filter.

Frequency tunability is achieved through the use of varactor diodes that are placed at the end of the  $\lambda/4$  open stub. The varactor diode serves to change the effective electrical length of the transmission line. Thin traces are then used to create a high impedance choke for the DC biasing of the varactor

diodes. For this design, GaAs abrupt varactor diodes from Cobham were used (MGV050-20), which have a typical junction capacitance of 0.48 pF with a tuning ratio of 2.6 [36].

Simulations were completed in Ansys® HFSS, where 0.2 pF capacitors were used to load the open stubs. Figure 30 shows the simulated insertion loss and the return loss with and without the resistor R. Without the resistor R, the filter is reflective when behaving as a BSF. However, when R is used, power is dissipated through it, resulting in absorptive or reflectionless characteristics. The resonant frequency of the simulated BSF is at 4.9 GHz. Figure 31 shows the return loss response at the resonant frequency when the value of R is changed. Maximum power dissipation of R occurs when the value is near 900  $\Omega$ .

Figure 32 shows the measured S21 and S11 response of the prototype BSF across various bias voltages. All of the varactors share the same bias voltage. Better than 20 dB of rejection is achieved from 3.96–4.4 GHz by tuning the varactor from 0–10 V. Also, from 3.5–4.5 GHz, the return loss is better than 8 dB, indicating that the BSF is well matched at all frequencies.

Finally, Figure 33 shows the correlation between the bias voltage and the resonant frequency, as well as the correlation between the 3-dB FBW and the resonant frequency. The frequency performance of this filter is mainly restricted by the limited range of the varactor diodes. The FBW can be improved by tuning the gap between the coupled lines in accordance to the normalized reactance slope in Equation 5.

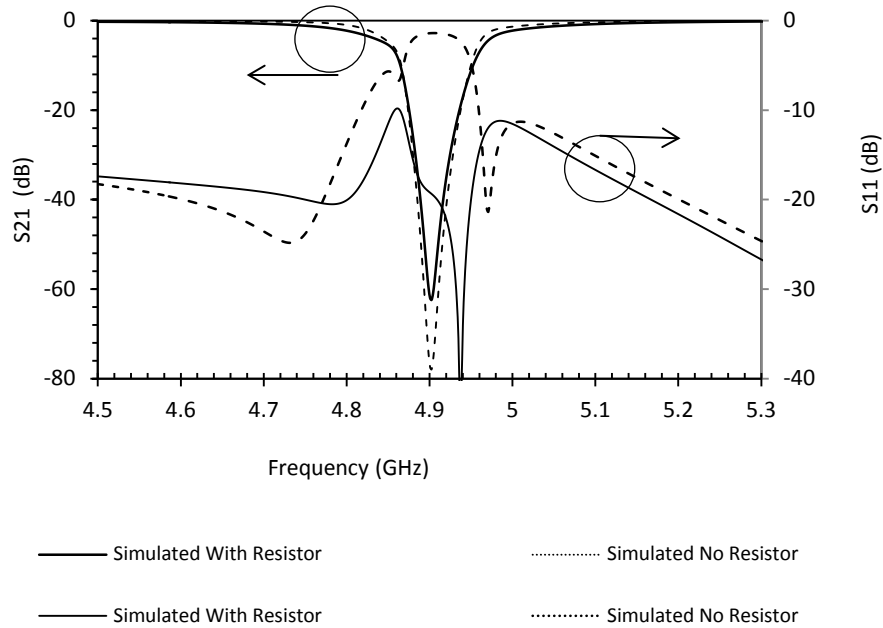


Figure 30. Simulated S21 and S11 of reflective and reflectionless designs.



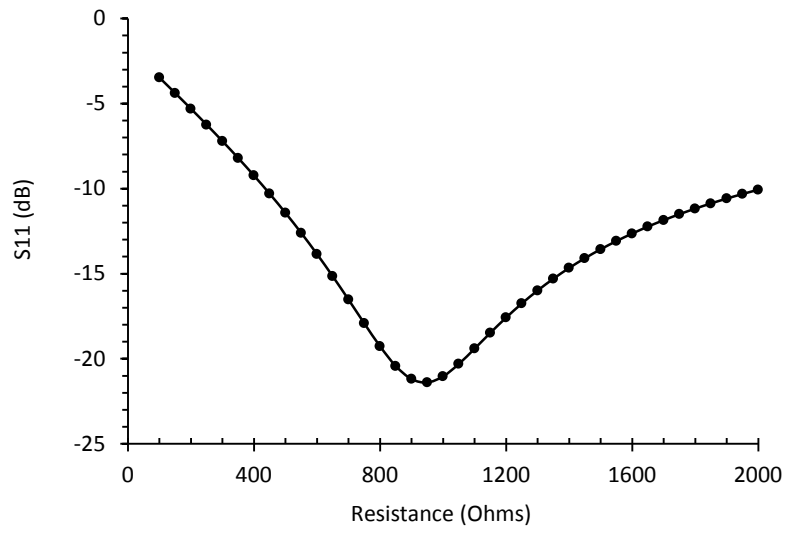


Figure 31.  $S_{11}$  at 4.9 GHz sweeping R.

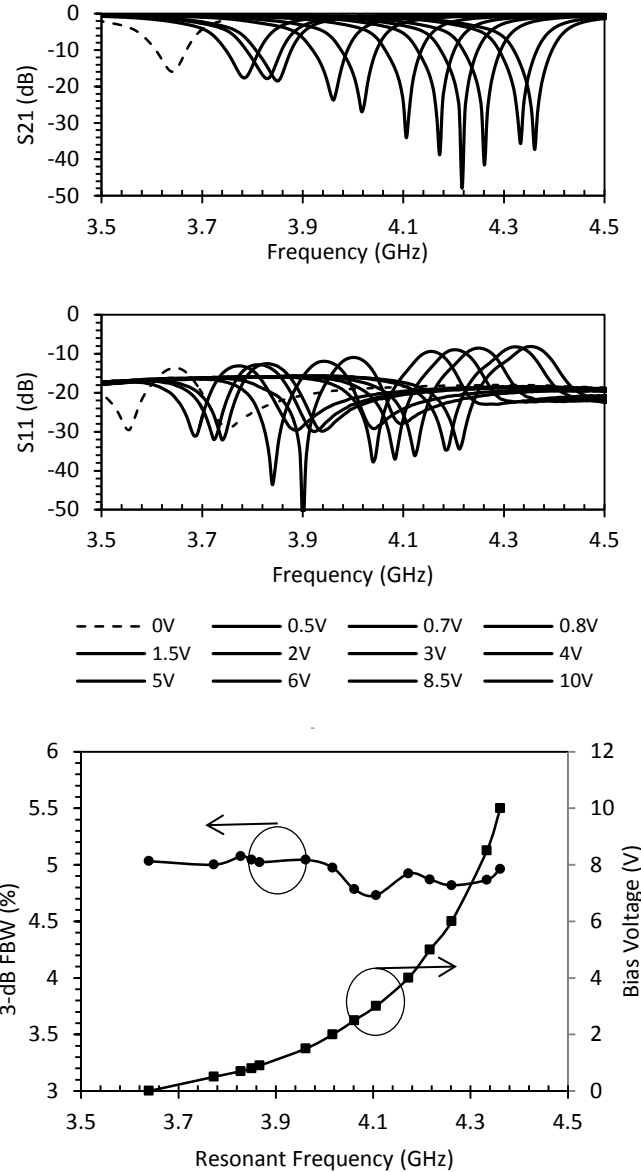


Figure 32. Measured 3-dB FBW, resonant frequency, and bias voltage.

#### 4.2.2 Quasi-lumped Element Design

BSFs are finding use in modern radios primarily because of the increased ubiquity of wideband systems. For example, many software-defined radios operate over wide swaths of bandwidth and as such are susceptible to performance degradation due to strong interferers. RF channelizers help provide a level of protection. However, the additional ability to precisely excise undesired signals is critical. Various BSFs have been recently investigated in references [25], [28], [37], and [38]; however, these are reflection type BSFs, and so the stopband attenuation is limited to the quality factors that can be realized in the resonators.

Recently, however, reflectionless type BSFs or absorptive BSFs have been proposed that overcome this basic limitation. Through the design of intentionally lossy resonators, reflectionless BSFs can achieve theoretically infinite attenuation. In reference [39] and reference [5], a

transmission line approach is presented that shows good performance around 1 GHz and 2 GHz respectively. Further demonstration is shown in references [9] and [30]. These early reflectionless designs were large in size due to the use of transmission lines. In references [11], [31], and [33], miniaturization is proposed through the use of an equivalent lumped element model. These designs are complex and require many lumped elements to realize. For low frequency applications in ultra high frequency (UHF) and below, these topologies may be applicable. But at frequencies beyond UHF, realization of these circuits can be difficult due to distributed parasitic and self-resonance effects from the numerous lumped elements. In reference [31] these are overcome by realization on an integrated circuit. However, in references [32] and [12], the authors have proposed a simple miniaturized lumped element reflectionless filter that is suitable for limited RF operation. The main drawback of this design is that as the quality factor and operating frequency changes the values of the resonators change with exception to the lossy resistors. In other words, the only way to increase the Q is to increase the values of the inductors used. This can be prohibitive at higher RF frequencies.

Therefore, we propose a new quasi-lumped element reflectionless filter topology in Figure 34 similar to Bode's original design in references [40] and [41] that minimizes the number of components, allows for more design flexibility in regards to component values, and still achieves large attenuation while maintaining a small size.

Much like in reference [39], our proposed topology uses phase cancellation to obtain high rejection. In this approach, two paths are introduced between the input and output ports and the signals are imposed to cancel each other by proper adjustment of the phase and amplitude. In this way, extremely deep notches can be realized using low-order resonators. To accomplish phase cancellation, an impedance inverter is typically used. In reference [39], two  $\lambda/4$  transmission lines are used; however, this constrains the size. In our proposed topology, the impedance inverter is a direct result of the bridge-T topology.

In Figure 34, the proposed notch filter is composed of a series bandpass resonator  $R_1L_1C_1$ , a bandstop resonator  $R_2L_2C_2$ , and a high-pass filter comprised of two series capacitors. The two resonators are designed to resonate near the same frequency. The high-pass section then acts like a delay or a phase shift, which is adjusted for optimal cancellation. Thus, when the input signal is "bridged" between the two passive circuit paths and both the resistance and reactance of the paths is equal, near infinite attenuation can be achieved [21]. A 5-GHz example design would result in:  $L_1=9.4$  nH,  $C_1=0.10$  pF,  $L_2=9.9$  nH,  $C_2=0.095$  pF, and a total delay of  $16^\circ$ . The values of  $R_1$  and  $R_2$  are determined through parametric simulation. This is shown in Figure 35. When  $R_1$  is  $2.25\Omega$  and  $R_2$  is  $20\Omega$ , the S11 and S21 are approximately -15 and -50 dB, respectively. High rejection is achieved while maintaining a good input match.

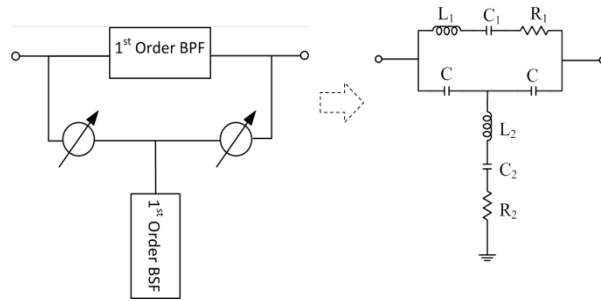


Figure 33. Proposed reflectionless bandstop filter.

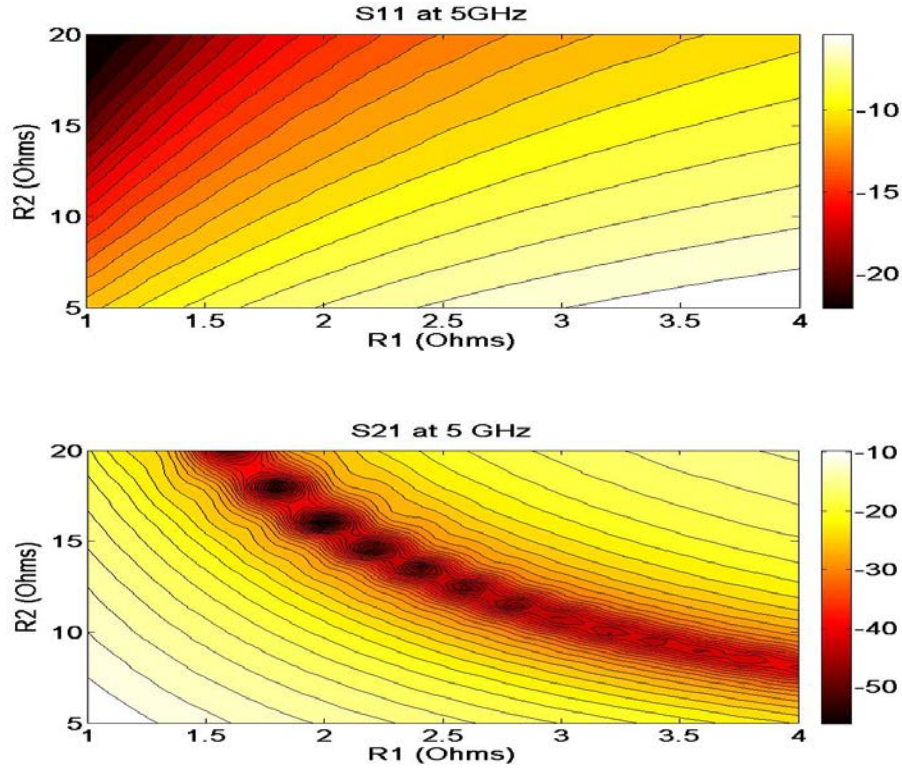


Figure 34. Contour plot of S21 and S11 when R1 and R2 are swept.

For this design, the C-Band was targeted, and at these frequencies surface mount resistors and capacitors are viable; however, most inductors have low self-resonant frequencies. For this reason, high impedance meandered transmission lines are used to provide the proper inductance. The fabricated prototype is shown in Figure 36, and the filter is implemented in microstrip on a 40-mil thick Rogers<sup>®</sup> 4350B substrate ( $\epsilon_r = 3.66$ ,  $\delta = 0.0037$ ). In this design,  $C_1$  and  $C_2$  are 0.1 and 0.2 pF, respectively. These are realized using AVX ACCU-P<sup>®</sup> capacitors.  $R_1$  and  $R_2$  are 7.5 $\Omega$  and 3.57 $\Omega$ , respectively, and are found parametrically. These are realized using Vishay<sup>®</sup> Dale CRCW0402 series resistors. Finally, the capacitor in the high-pass filter,  $C$  is set to 4.7 pF. This is realized using Vishay<sup>®</sup> RFCS series capacitors. Sonnet was used for all electromagnetic simulations on the filter structure with S-parameter models for each component.

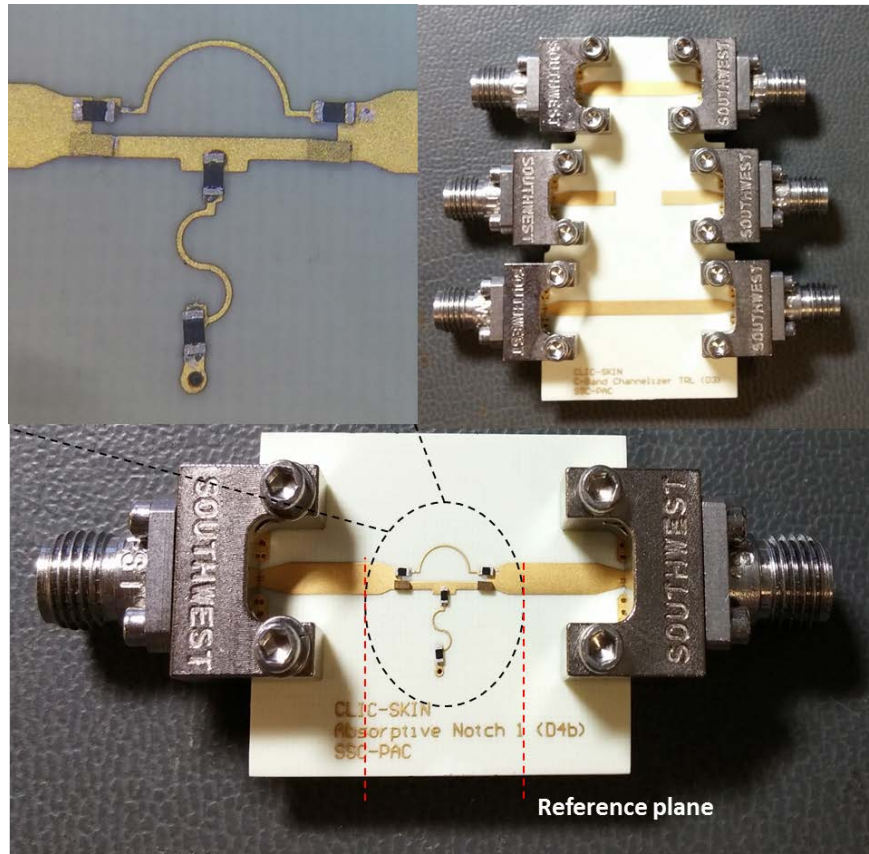


Figure 35. Fabricated fixed frequency prototype and TRL calibration substrate.

The prototype was measured using coaxial edge connectors from Southwest Microwave, Inc., and a custom TRL calibration substrate is used to de-embed the measurements to the reference plane shown in Figure 37. The measured and simulated results are shown in Figure 37, and the correlation is good. The measured rejection is over 50 dB at 4.1 GHz, and the return loss is better than 6 dB over the whole band of operation. The measured 3 dB and 10 dB bandwidths are approximately 1 and 0.25 GHz, respectively. The measured 10-dB percentage bandwidth is therefore 6%. The measured insertion phase is shown in Figure 38 and shows that at the cancellation frequency, the signal goes through near  $180^\circ$  phase change.

Frequency tunable notch filters are also quite desirable. Our proposed architecture is capable of supporting this with the simple addition of varactors in place of C1 and C2, and high impedance bias lines. We used the Cobham<sup>®</sup> MGV050-18 GaAs abrupt varactor diode to test the tunability. This diode has a junction capacitance (CJ) of 0.41 pF and a tuning ratio of 2.0. Figure 39 shows the fabricated frequency tunable prototype. Since the overall capacitance when using the varactor is greater than the fixed frequency design, we would expect that the frequency of operation to be shifted down. Figure 40 shows the measured results under four different bias voltages. The notch filter can be tuned from 2.51–2.83 GHz with a rejection of better than 20 dB. In this design, each varactor requires its own bias voltage.

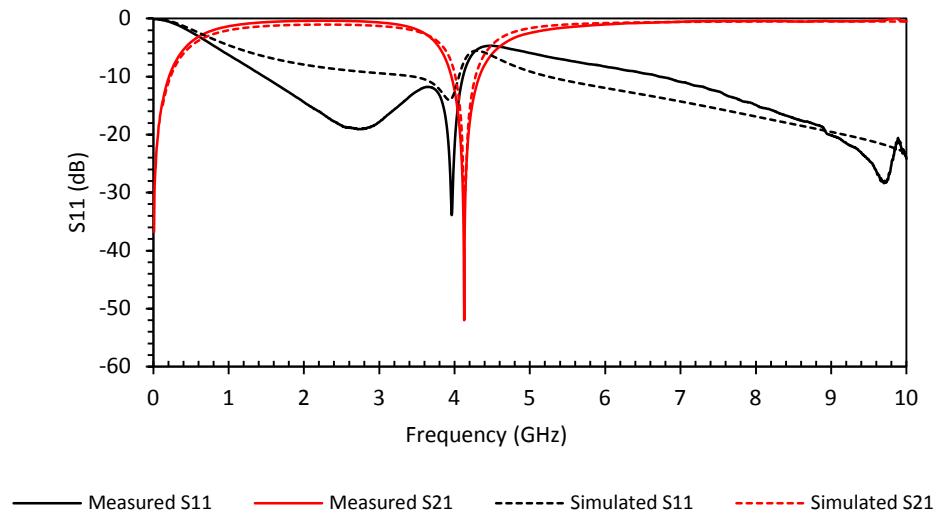


Figure 36. Measured and simulated S11 and S21.

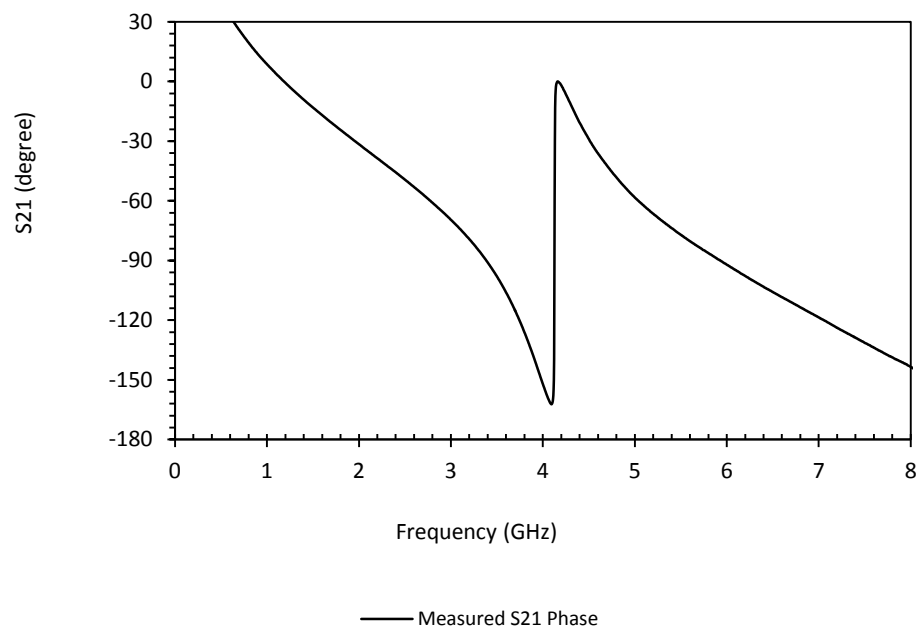


Figure 37. Measured S21 phase.

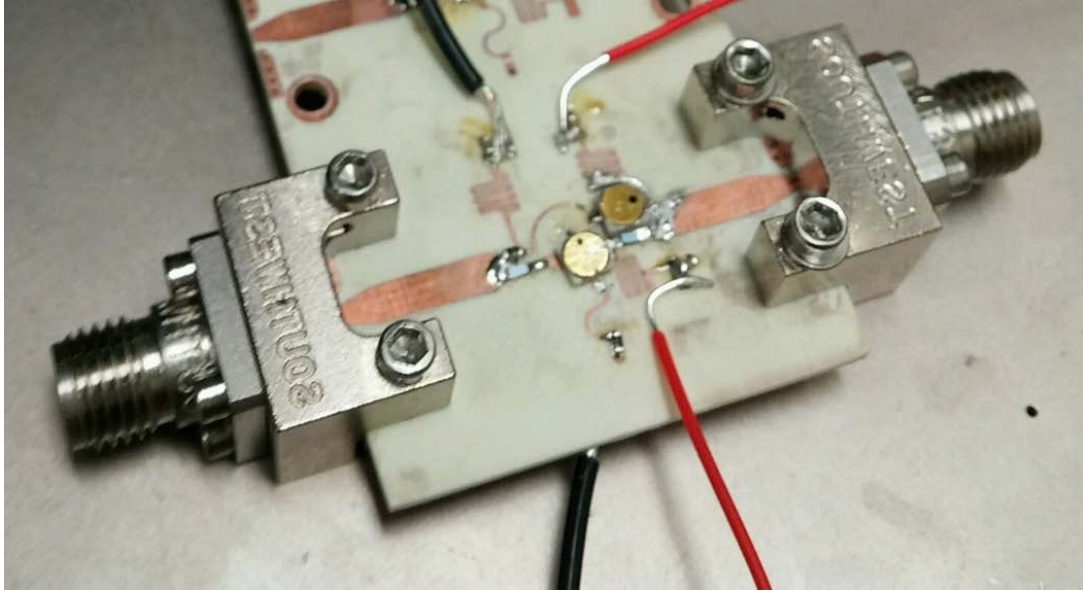


Figure 38. Fabricated frequency tunable prototype and calibration substrate.

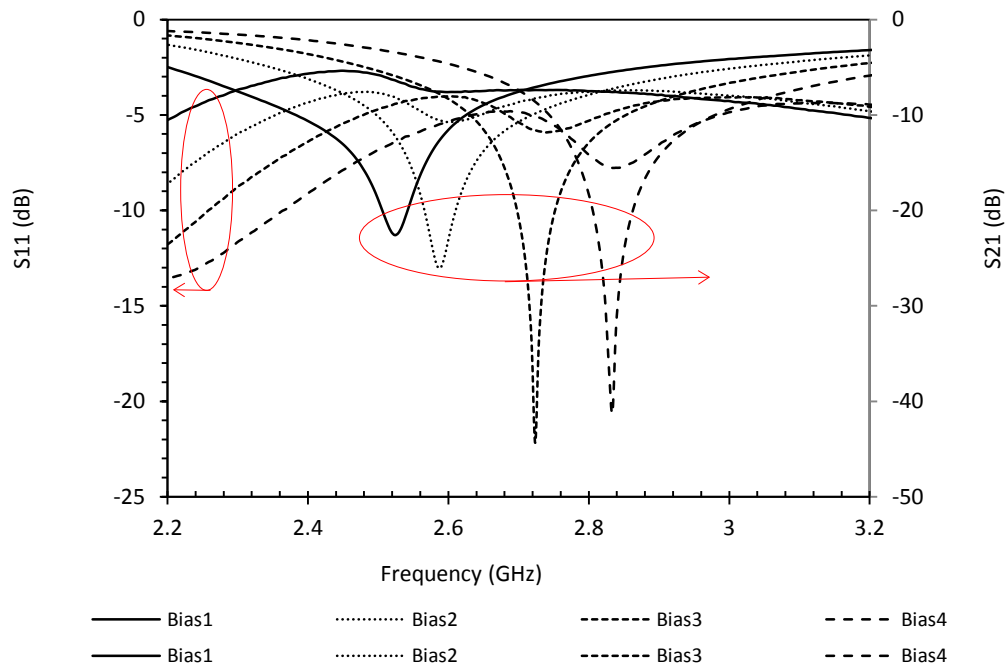


Figure 39. Measured frequency response of tunable prototype.

#### 4.3 INTEGRATION OF RF CHANNELIZER WITH TUNABLE NOTCH FILTER

At the end of the first year of the study we tried to integrate one of our designed notch filters with the five-channel channelizer. The ultimate approach was to incorporate a tunable notch filter for each of the channels. In this approach, each notch filter was designed and optimized to cover the entirety



of each channel. However, because of time considerations in the first year we simply demonstrated this concept with a single channel instead of all five. In the second year, we demonstrated in the X-band and anticipated having tunable notch filters for each channel. Figure 41 shows the fabricated prototype incorporating both a tunable notch filter with the channelizer. For this design, the edge-coupled transmission line absorptive notch filter (Section 3.2) was used because the achieved quality factor was higher, creating a more selective BSF with a narrower stopband. The designed prototype operates such that the tunable notch filter covers channel one, from approximately 3.5–4 GHz.

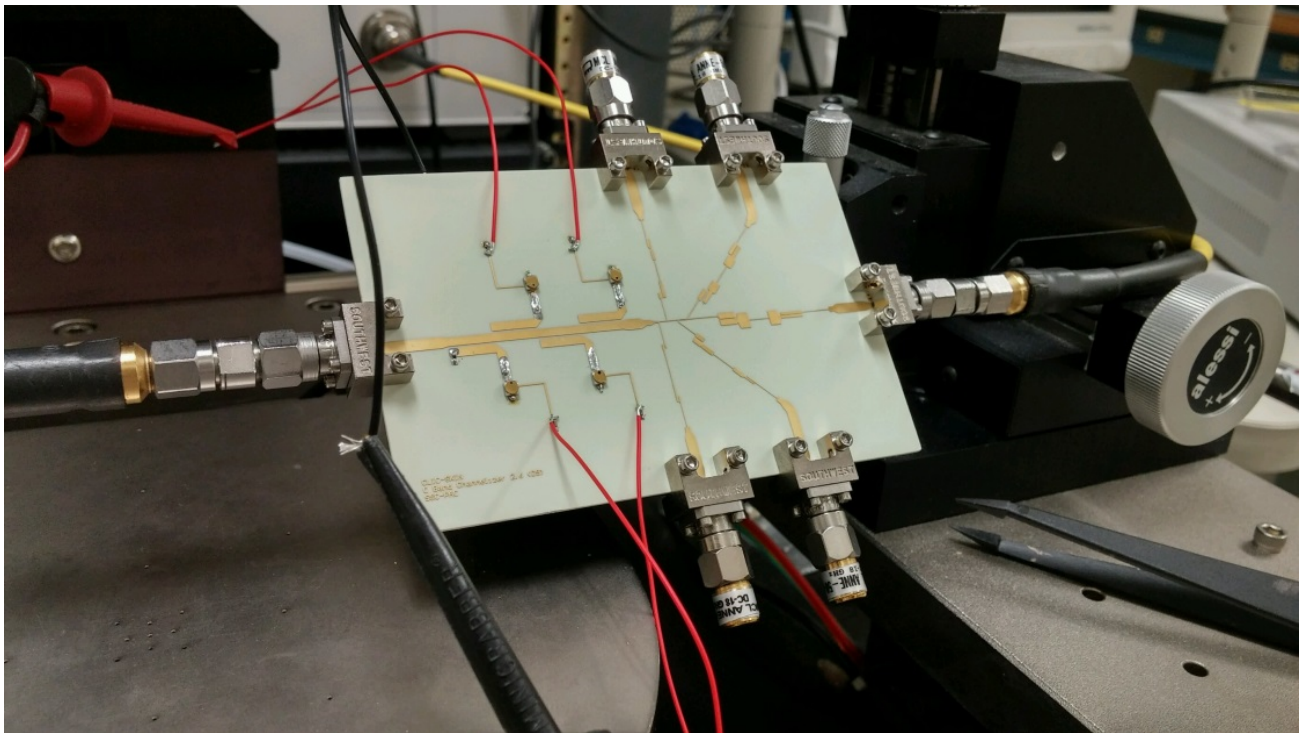


Figure 40. Prototype CLIC-SKIN for C-Band.

Figure 42 shows the measured results of the channelizer with an embedded tunable notch filter. The notch can be tuned arbitrarily within the passband of channel one with approximately 5% fractional bandwidth. To create a narrower notch, more stages can be cascaded with the penalty of incurring a higher insertion loss. Shown in Figure 42 in the absorptive regime, the notch filter gets more than 40 dB of rejection. The ability to channelize the frequency regime that a radio operates in offers a first level of protection to the front end amplifier. Using only channelization, if a strong interferer enters one of the passbands that passband can be sacrificed with the rest of the channels remaining fully operational. With the addition of a tunable notch filter that is embedded into each channel filter, this adds an extra level of protection, possibly saving portions of the channel instead of sacrificing the entirety of the channel. Figure 43 and Figure 44 show the fabricated prototype printed circuit board for all of the test structures for year one.



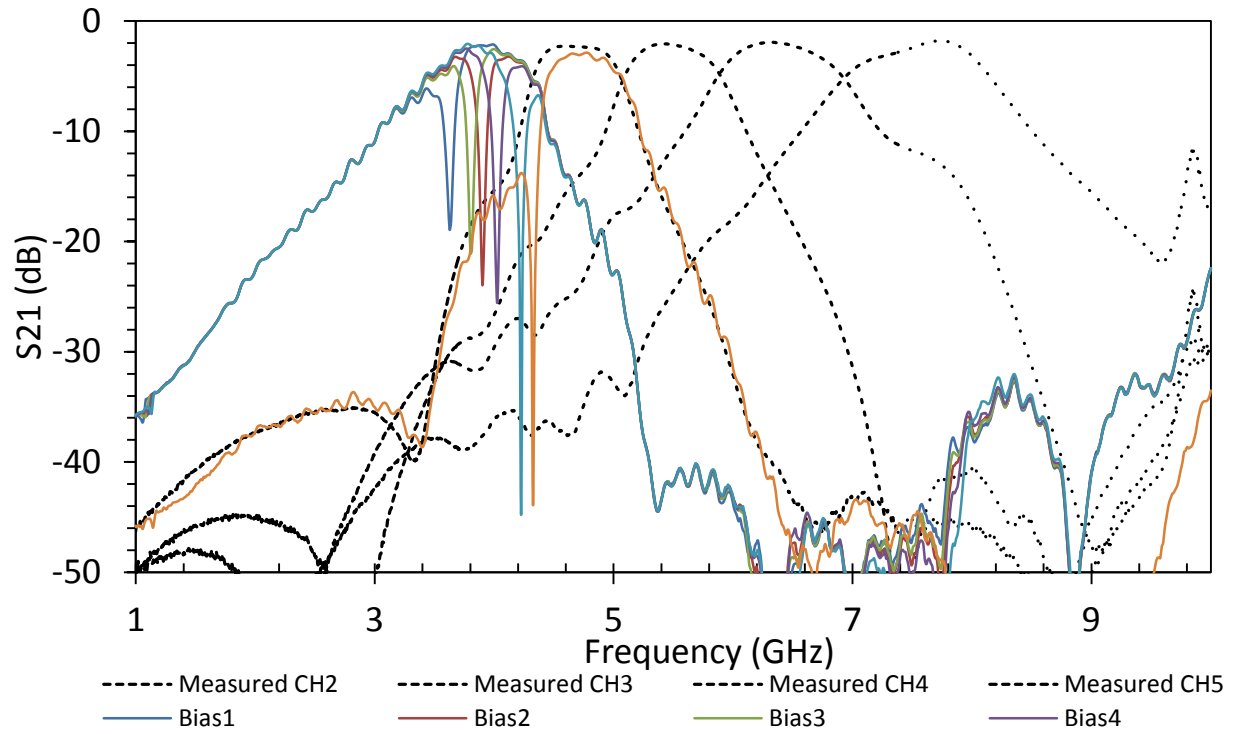


Figure 41. Prototype CLIC-SKIN for C-Band.

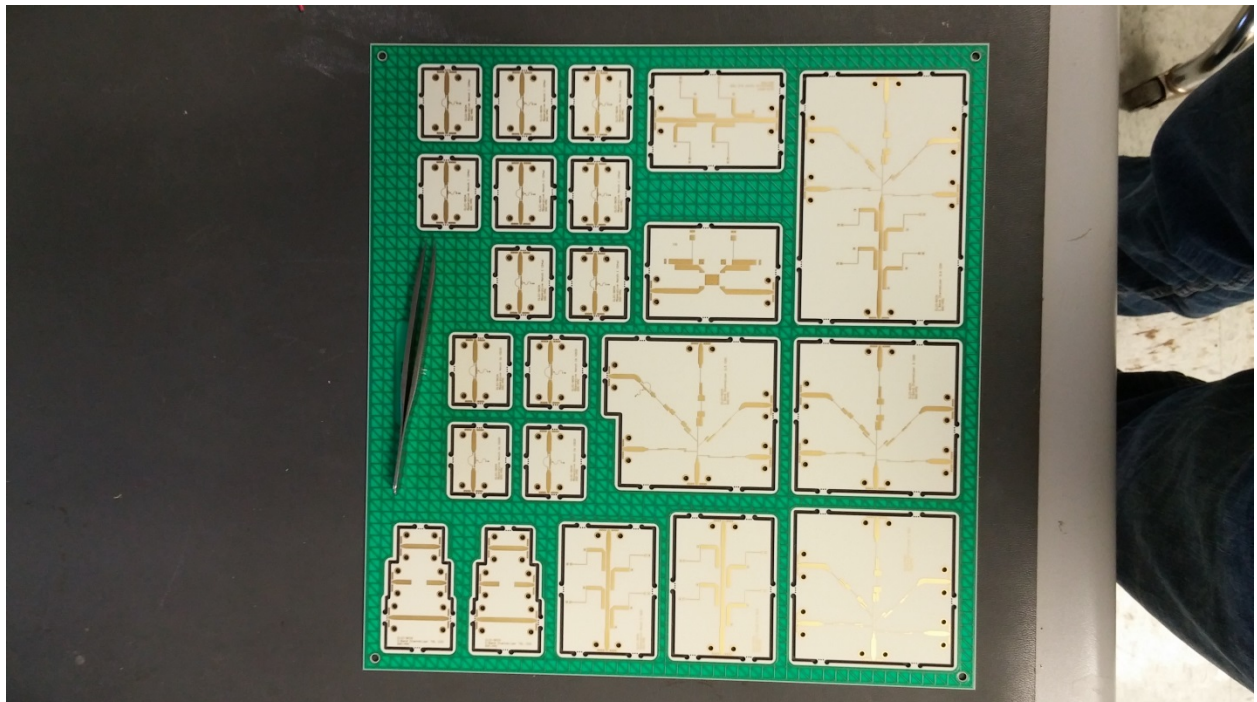


Figure 42. Printed Circuit Board Fabrication for absorptive bandstop filters, RF Channelizers, and CLIC-SKIN.

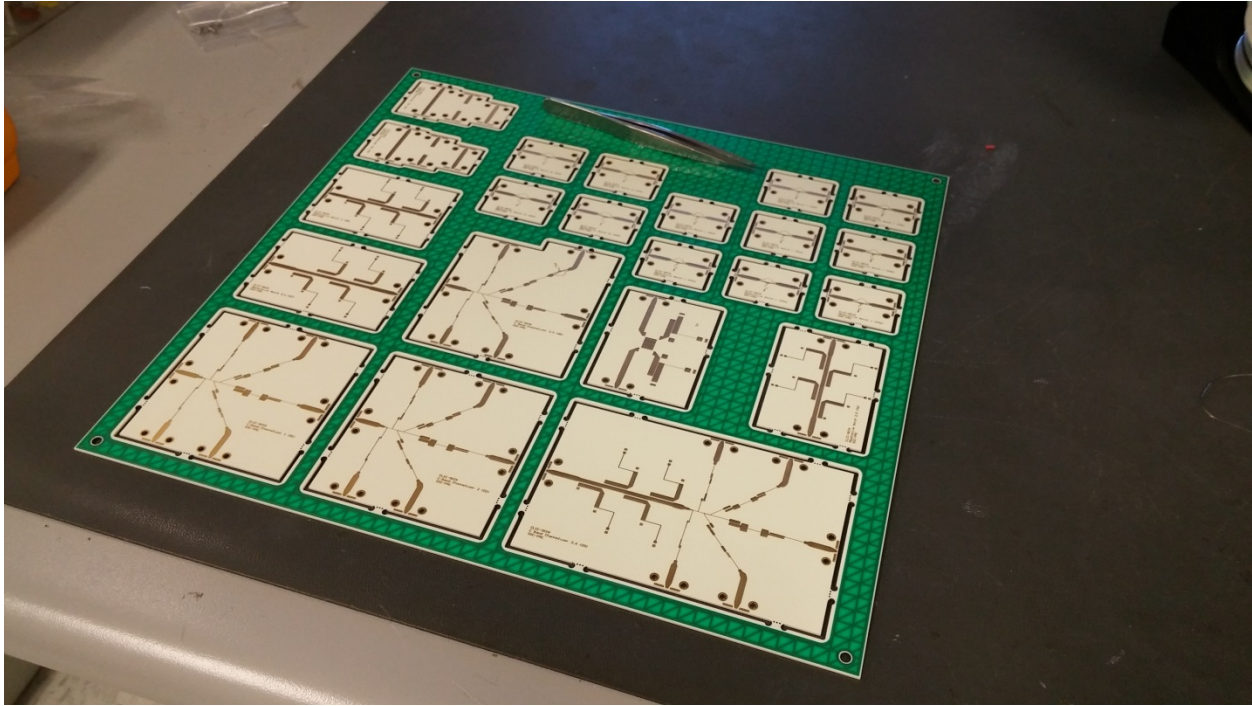


Figure 43. Printed Circuit Board Fabrication absorptive bandstop filters, RF Channelizers, and CLIC-SKIN.

#### 4.4 COMPARISON WITH PHOTONIC TECHNOLOGY

Although this project aims to develop microwave channelizers and BSFs for interference mitigation using traditional microwave circuit design techniques, an equally significant approach to this task is through the use of photonic technologies. In reference [42], signals are converted into the optical domain and interference mitigation BSFs are demonstrated. In reference [43], a phase cancellation approach is taken much like reported in Section 3.2, although in the optical domain. This reported filter has the unique capability to maintain a very low percent bandwidth (although the definition of how % bandwidth is defined is not reported), and tune through a broad range of frequencies while maintaining a high level of rejection. This type of filter looks very promising. Things that are not reported in reference [44] are the optical to analog loss/gain that the system incurs. Typically, there is a conversion such that the RF/analog signal can be processed in the optical domain. The efficiency of this type of conversion can limit its adoption. In reference [45] the reported attenuation with optical to RF conversion is  $> 25$  dB, up to 35 dB. This loss will need to be compensated for in the RF analog domain with a broadband amplifier. OE Waves, Inc. has also explored this topic and published its results in reference [46].

A comparison between some published works on microwave notch filters are presented in the Table 3. Although photonic technologies can attain a wider tuning range and a narrower % bandwidth [43], the cost can be prohibitive as system development would require using photonic lasers as well as optical to RF converters. The size and ability to integrate would also be a limitation, as most microwave and RF systems are implemented using traditional circuit board technology. As optoelectronics progresses and the ability to integrate on a board level becomes a possibility, it is anticipated that photonic technologies will become more widespread.

Table 3. Comparison between some published works on microwave notch filters

Works	Center Frequency	Tuning Range	% Bandwidth	Rejection	Cost
Reference [42]	1.5 GHz	-	1	> 50 dB	\$\$\$
Reference [43]	-	1 – 30 GHz	0.05% - 0.2%	> 60 dB	\$\$\$
Reference [44]	7.1 GHz	-	3.5%	> 60 dB	\$\$\$
Reference [45]	-	2-8 GHz	4.12%	> 55 dB	\$\$\$
Reference [46]	-	-	10 MHz	> 45 dB	\$\$\$
This work (coupled lines)	-	3.6 – 4.3 GHz	~5%	> 55 dB	\$ (\$50)
This work (quasi-lumped)	4.12 GHz	-	25%	> 55 dB	\$ (20)

## 5. TECHNOLOGY DEVELOPMENT IN X-BAND

The objective of the second year of the study was to develop a RF channelizer with a built-in tunable notch filter that is capable of supporting bent-pipe SATCOM systems, notionally in the X-band. This project will follow the aforementioned project description and corresponding technical approaches.

Wideband radios are becoming more widespread as software-defined radios and multi-function RF become ubiquitous. Wide bandwidths allow for operational agility but often are more susceptible to blocking from a strong interferer [25]. In many of these wide bandwidth microwave systems, the LNAs are the most sensitive component. High-power interference or jammers can push the LNAs into compression, blocking the receiver, and in some instances can damage the front end. In many instances, LNAs with limiters are employed to protect the receiver; however, most solid state limiters are not frequency selective and therefore short the input even if a very narrowband high power signal is present.

A more preferable solution is to develop frequency-selective limiters that can protect a wideband RF front end. One recent example of this is in reference [47], where a switched multiplexer is used. We propose a different topology using a two-tiered approach. The first level of protection is through the use of a frequency multiplexer or channelizer to parse the wide full bandwidth into smaller channels. The second level of protection is through the use of tunable notch filters embedded into each channel filter. These tunable notch filters can excise high-power interferences precisely, which allows for frequency selective limiting. Since high levels of rejection are required, absorptive BSFs were used to achieve high cancellation using low-order resonators [5; 17; 26]. This also serves to dissipate unwanted signals instead of reflecting them back through the antenna. Figure 45 shows the proposed concept. This type of architecture is especially suitable for interference mitigation from co-located frequency hopping radios. If the hopping scheme is known a priori, then the tunable notch filters could be set accordingly to deconflict when co-site interference falls within the same subchannel.

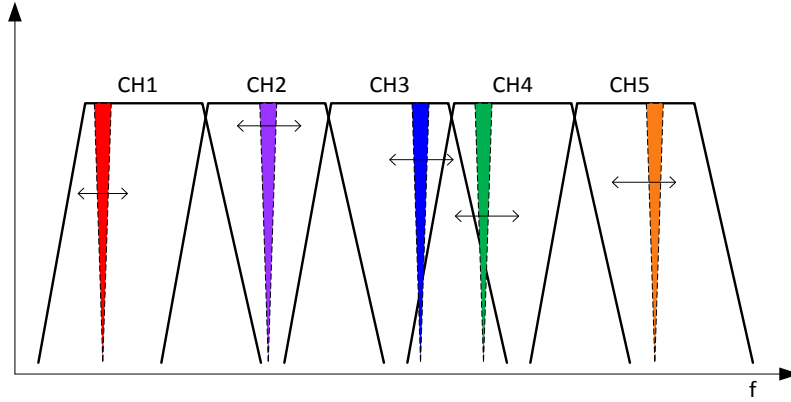


Figure 44. Channelizer with embedded tunable notch filters.

### 5.1 DEVELOPMENT OF COCHLEA CHANNELIZER

As described in Section 4.1, the Cochlea channelizer is preferable because high-frequency channel filters are closer to the input of the filter, mitigating insertion loss, which is more deleterious at high frequencies. To generate the series inductance and capacitances necessary for the tubular filters, micro-fabrication was used instead of printed circuit board fabrication. We used Applied Thin Films (ATP) for thin film deposition. For X-band, since substrate loss can be high at microwave frequencies, a fused silica (quartz) substrate was adopted. Metal deposition resolutions of better than 20  $\mu\text{m}$  can be achieved using thin films, much better than in printed circuit board processes. A five-channel channelizer was designed as part of this effort, following the same design procedures described in Section 4.

The prototype channelizer was fabricated on 20-mil fused silica quartz substrate ( $\epsilon_r=3.8$ ,  $\delta=0.00006$ ). An inductive manifold couples to each channel filter forming an up-converting ladder network. A tubular type filter is used to achieve the specific behavior required by the channel filter. Typically, the tubular channel filters are realized using lumped elements. However, at microwave frequencies, this is not possible because of low self-resonant frequencies of surface mount inductors and capacitors. Instead, transmission line equivalent circuits are adopted as in reference [4]. Series inductors are realized as high impedance transmission lines. Series capacitors are realized using edge coupled transmission lines. Shunt capacitors to ground are realized using wide transmission lines that have a parallel plate capacitance to ground. Minimum feature size of the channelizer are the edge coupled transmission lines, which have a gap size of 1 mil. Each channel filter was designed for ~15% fractional bandwidth across the center frequency. Figure 46 shows the measured performance of the channelizer across the five channels, and also shows the fabricated prototype in the inset. The insertion loss on channel three deviates from simulation, and this is attributed to fabrication tolerance of the edge coupled lines, which are critical. The average insertion loss is around 3 dB for the entirety of the channelizer, and adjacent channel rejection is over 9.8 dB from channel center.

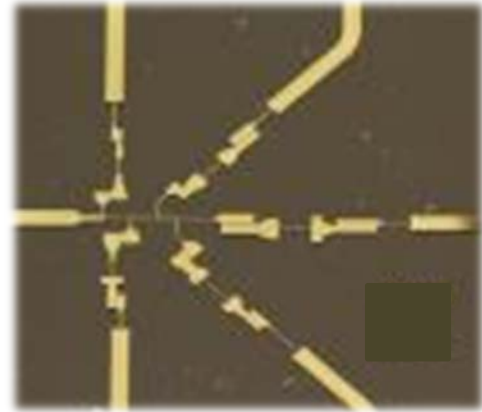
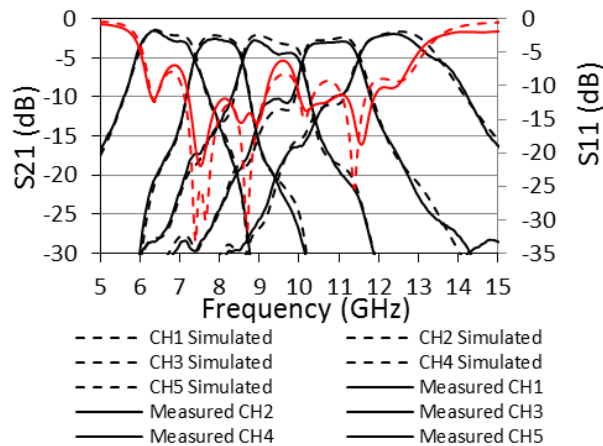


Figure 45. X-band 5 contiguous channel frequency multiplexer designed on 10-mil fused silica.

## 5.2 DEVELOPMENT OF ABSORPTIVE BANDSTOP FILTER DESIGN

Absorptive bandstop filters (ABSF) have the capability of achieving high rejection using low quality factor (Q) resonators [9], [48]. A transmission line realized two-path notch filter is used. The input signal is coupled through a BPF to the output, while a portion of the input signal is coupled through a BSF to the output. The two portions are phased such that at the designed frequency of the two paths are  $180^\circ$  out of phase, resulting in near perfect cancellation. Flip chip varactor diodes (MAVR-000102-1441) are used to load the BPF and BSF in order to make the two filters tunable. Radial stubs are used for bypass capacitors and  $\lambda/4$  transmission lines are used as chokes for DC biasing.

Five separate ABSF filters are designed for each of the five channels. Each one is designed for around 4% fractional bandwidth around the center frequency and with the capability to tune across the full bandwidth of each channel. Figure 47 shows the fabricated prototype for the ABSF for channel 2. Measurements are done using GSG probe launches with a custom TRL calibration kit to de-embed the effects of the probe launch. Figure 48 shows the measured performance of the ABSF, showing more than 35 dB of attenuation from 6.6–7.5 GHz with a 3-dB bandwidth of around 170 MHz. The varactor diodes are swept from 0–10 V and are designed to be swept simultaneously with the same voltage. The filters were also designed on a 20-mil fused silica-quartz substrate.



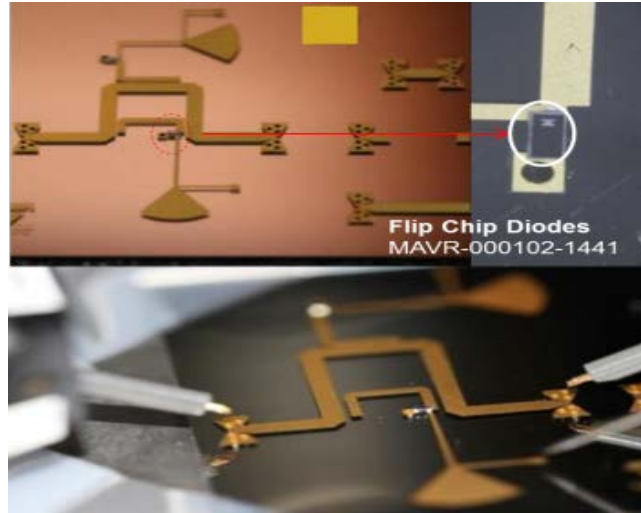


Figure 46. Fabricated prototype of absorptive tunable bandstop filter for channel 2.

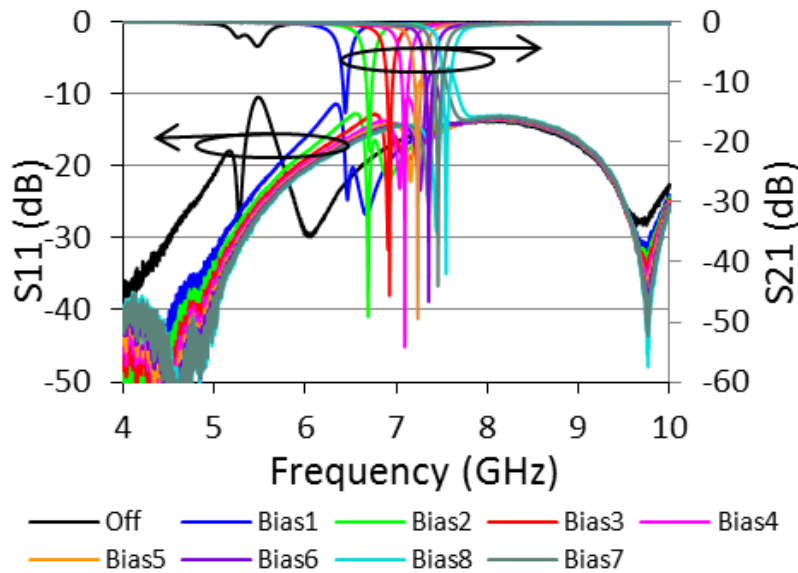


Figure 47. Measurement result of ABSF for channel 2.

### 5.3 DEVELOPMENT OF FREQUENCY SELECTIVE MULTIPLEXER LIMITER

Figure 49 shows the completed frequency selective limiter using the channelizer developed from Section 5.1 and the tunable ABSF from Section 5.2. Flange-mounted SMA connectors were used for measurement purposes, and DC EMI filters were used to provide voltage biasing to the circuit. The total size of the prototype is 2.7 inches by 2.7 inches. Figure 50 shows the measured response for channel one with the ABSF tuned to various frequencies. More than 12 dB of rejection is achieved across the full band, with more than 40 dB at its peak.

To test the performance of the prototype, the test setup in Figure 51 was used. A signal of interest was injected into channel 1 with a center frequency of 6 GHz using 16 quadrature amplitude modulation (QAM) with a symbol rate of 8 Msym/sec and an output power of -55 dBm. A high-power jammer was also injected into channel one using a power combiner, with a center frequency of

6.9 GHz at an output power of +11 dBm. These signals were fed into the frequency selective channelizer limiter preceding a LNA (AML-2014307-001). An Agilent® E4440A was used as a digital receiver, demodulating the digital signal. When the ABSF was turned off, the jammer saturated the LNA, preventing the digital signal from being received, the maximum peak error vector magnitude (EVM) was measured to be 95%. The power level of the jammer was measured to be +14.88 dBm at the receiver. When the ABSF was tuned to 6.9 GHz, the jammer was suppressed by more than 33 dB and the constellation is recoverable. The measured maximum EVM was reduced to 57%. This is shown in Figure 52. Phase and amplitude errors resulting from the instrumentation/test setup is attributed to high general EVM. Figure 53 shows the full frequency response of the entire five-channel X-band channelizer with embedded tunable absorptive notch filters. The slight amplitude ripples in the measured channel response is attributed to poor electrical contact between the fused silica substrate and the housing/case, which was bonded through the use of silver epoxy.

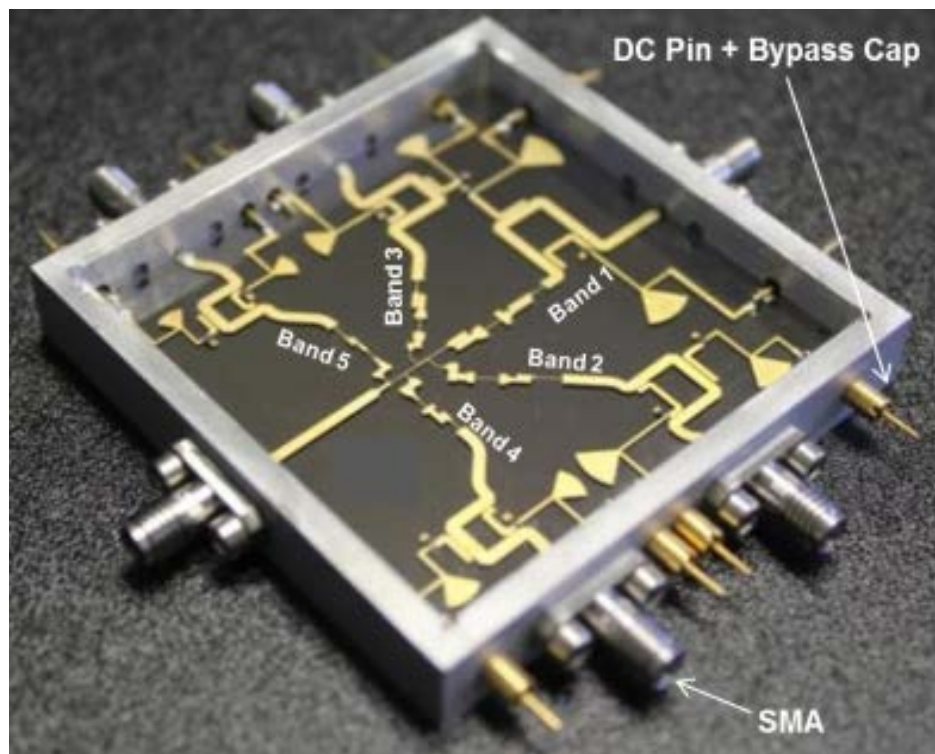


Figure 48. Prototype of X-band frequency selective limiter using absorptive tunable notch filters embedded multiplexers. Prototype is 2.7 inches by 2.7 inches.

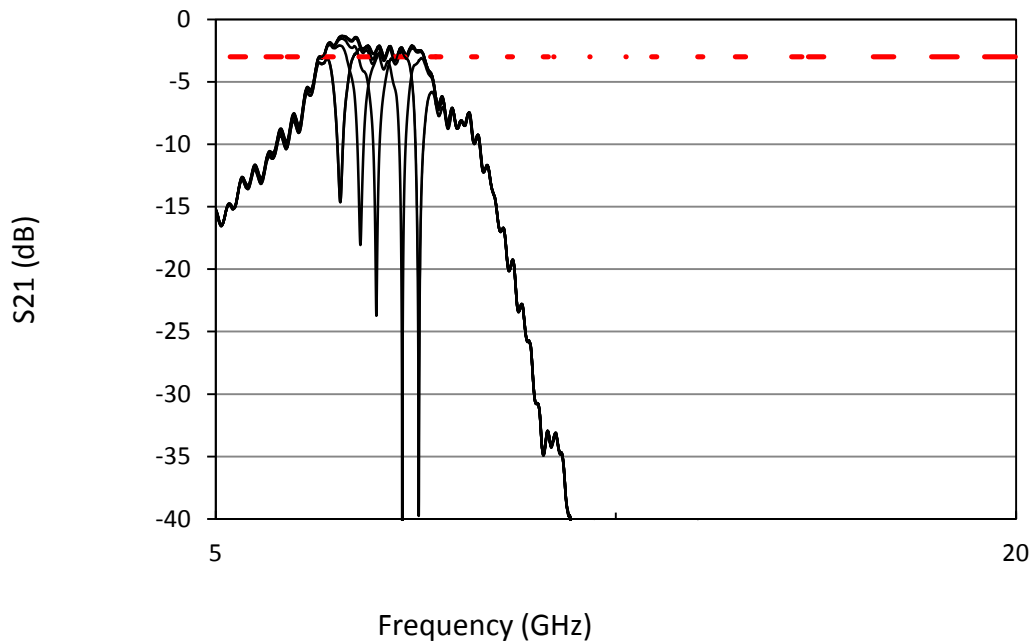


Figure 49. Channel characteristics of channel one with tunable notch filter (red line indicates 3dB).

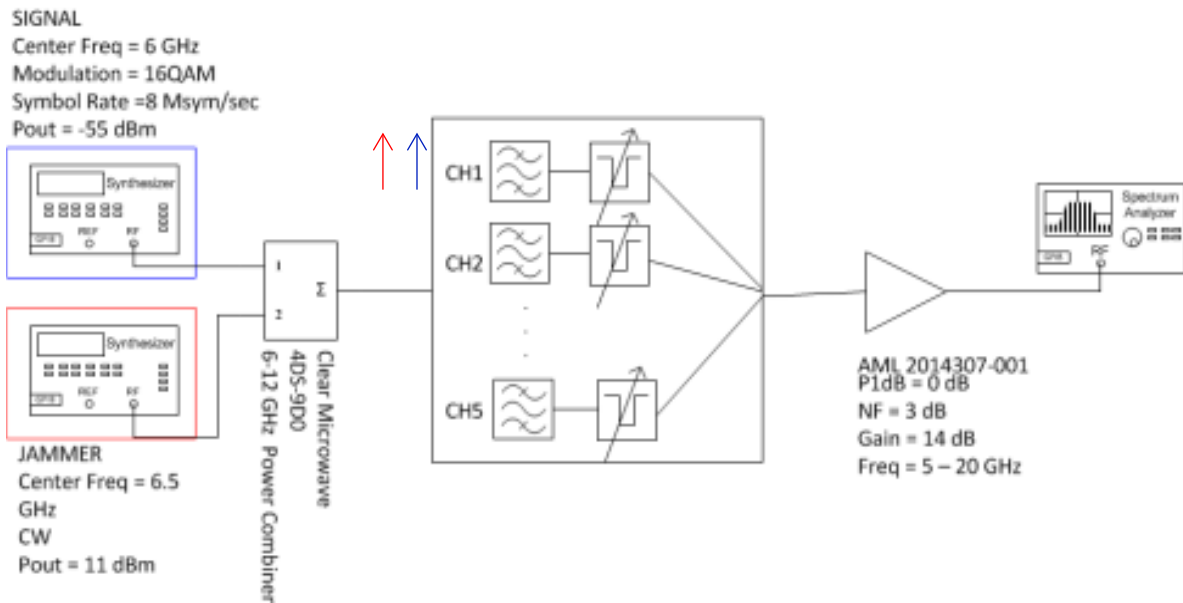


Figure 50. Test use case setup for co-channel narrowband interferer.



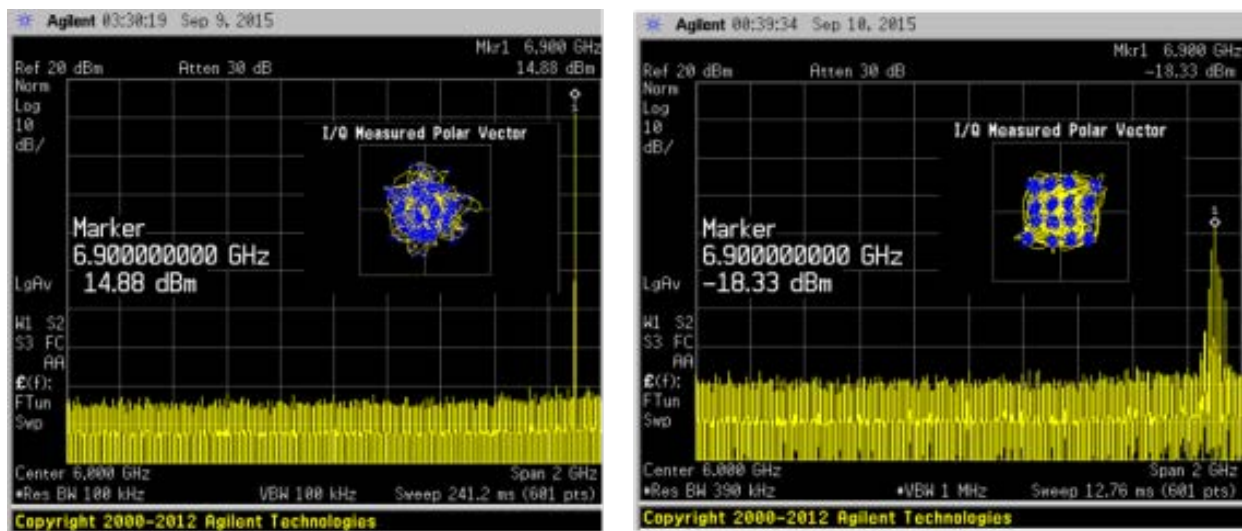


Figure 51. Measurement results before (left) and after (right) ABSF is tuned to blocking signal.

## Channelizer + ABSF

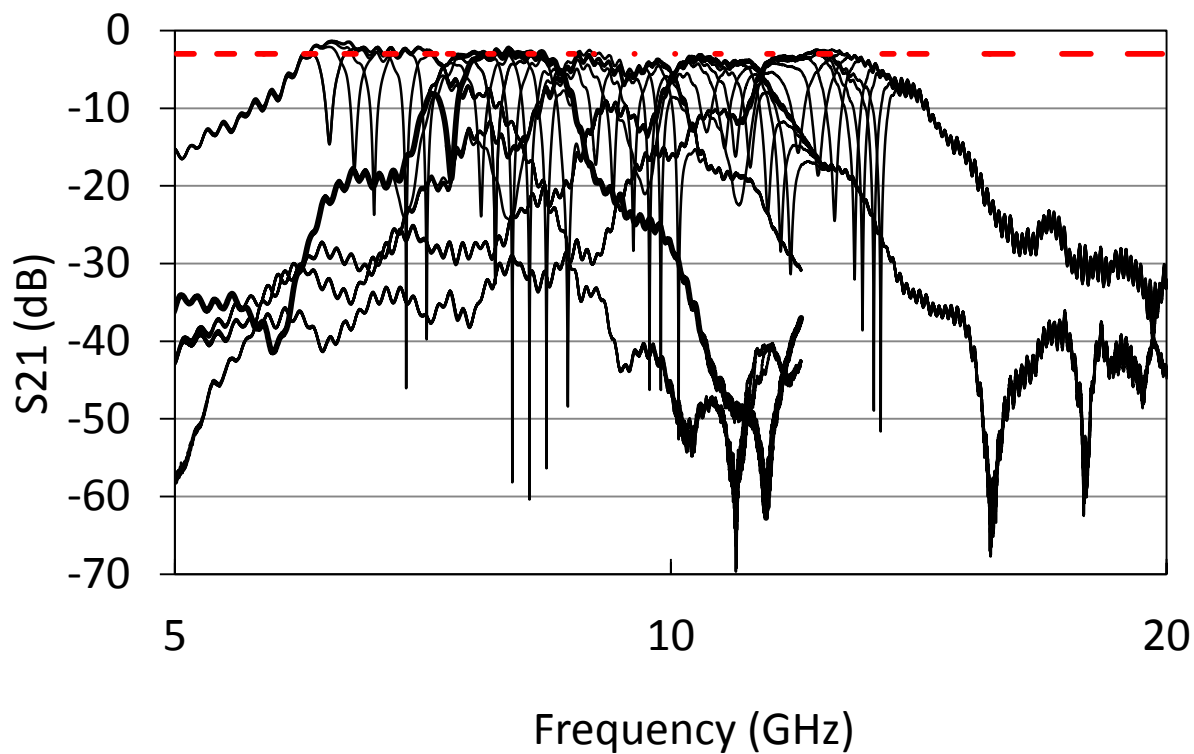


Figure 52. Full frequency response of the five-channel channelizer with embedded absorptive tunable notch filters.

Some other test cases were also examined as part of the project. Figure 54 shows an example of a test case when the RF front end is wide open and susceptible to jamming. Figure 55 shows the response before and after a high-power signal is presented in far proximity to the signal of interest. When the jammer is introduced, even though far in frequency from the signal of interest, the jammer saturates the LNA and the receiver is no longer able to demodulate the signal. Figure 56 shows the test case when a close in jammer is presented, and Figure 57 shows the measured results. As expected, the wide open RF front end is saturated and the signal of interest is no longer able to be demodulated. Figure 58 shows a final test case where a channelized receiver is used, the signal of interest resides in channel 1, and a jammer is presented in channel 2. Because of the roll-off response of the channel filters, the RF front end in channel 1 is protected from the jammer in channel 2. The introduction of the jammer does not degrade reception of the signal of interest. Figure 59 shows the results.

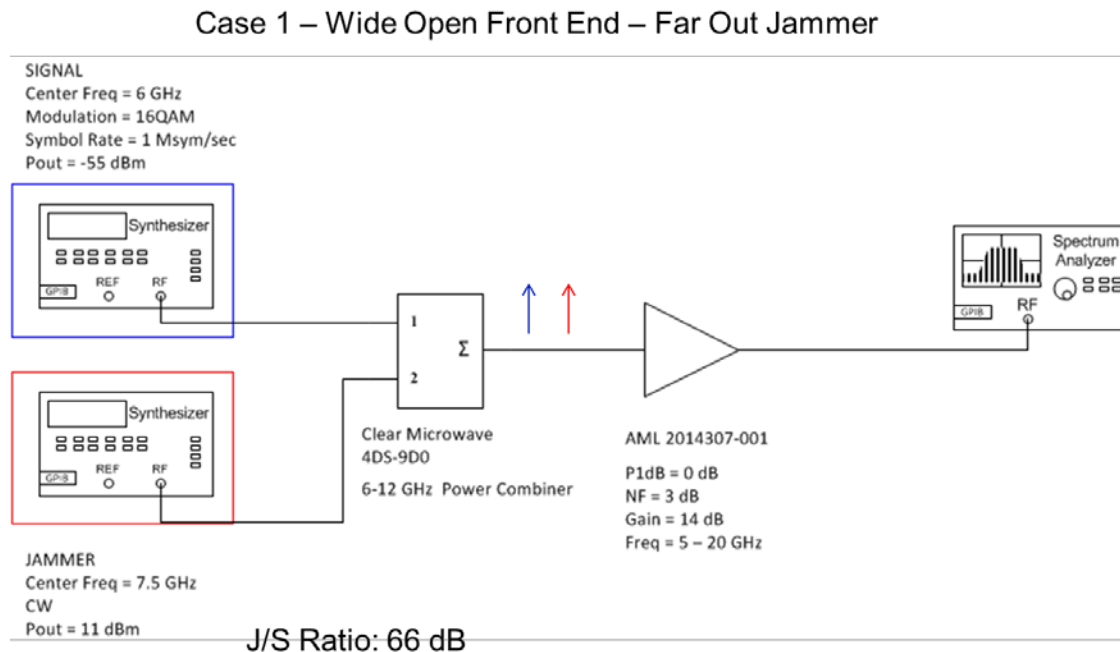


Figure 53. Test case for wide open RF front end for far out jammer.

## Case 1 – Wide Open Front End – Far Out Jammer

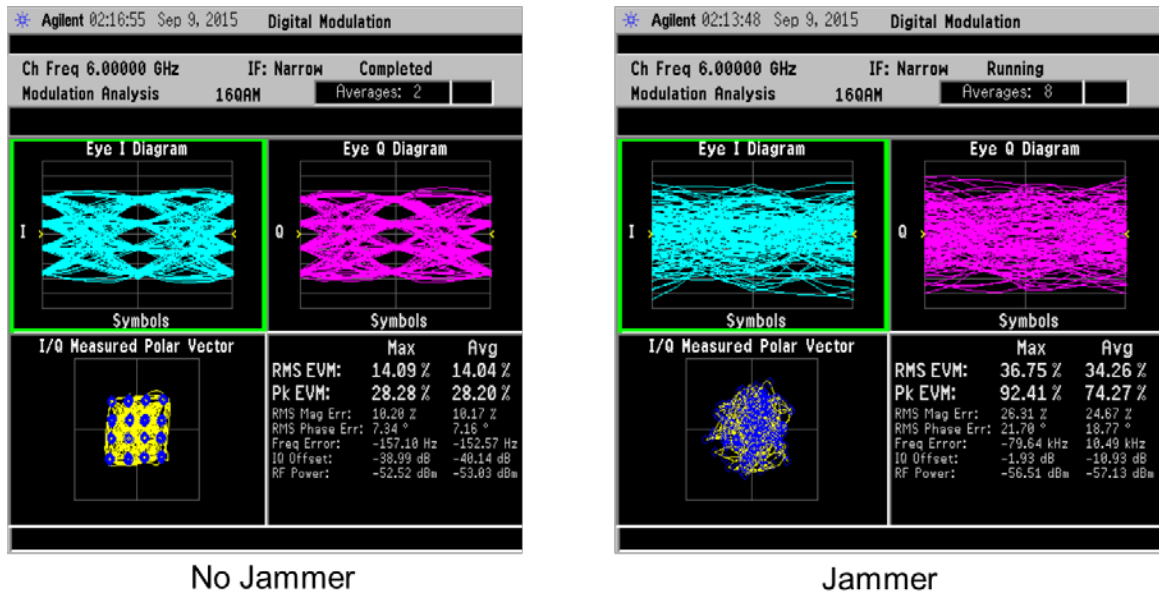


Figure 54. Response of the receiver before and after a far out jammer.

## Case 2 – Wide Open Front End – Close In Jammer

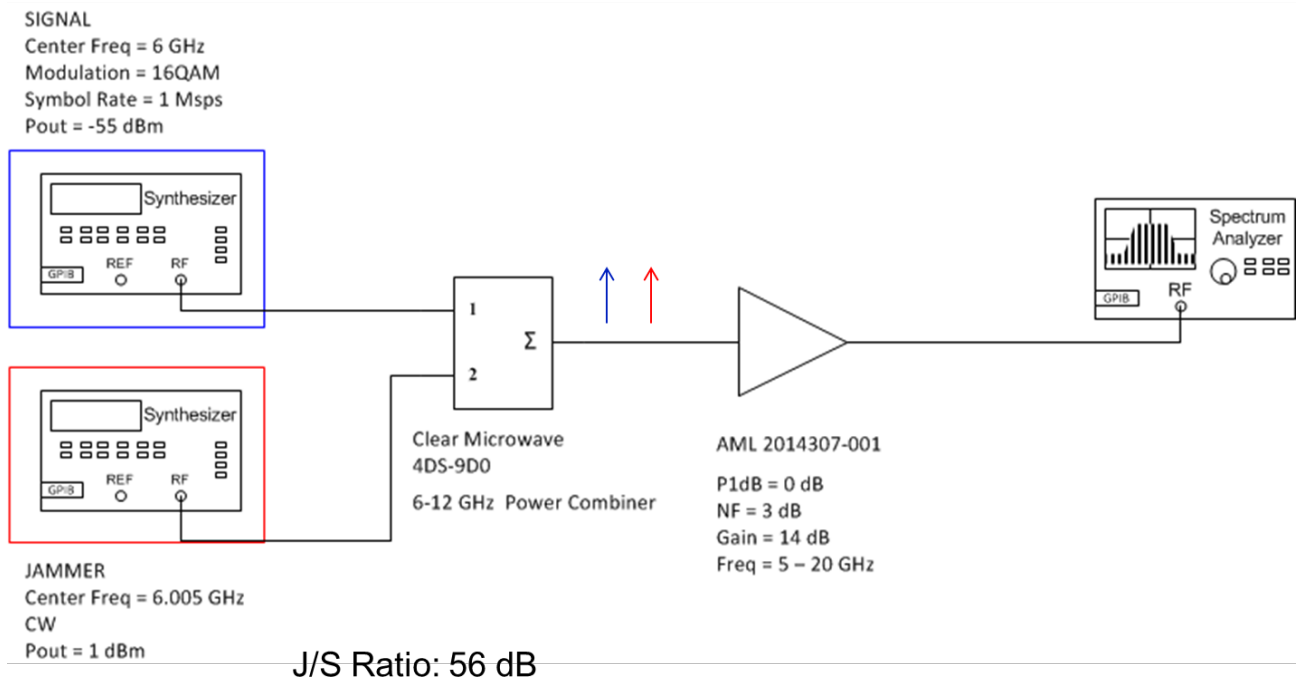


Figure 55. Test case for wide open RF front end close in jammer is presented.

## Case 2 – Wide Open Front End – Close In Jammer

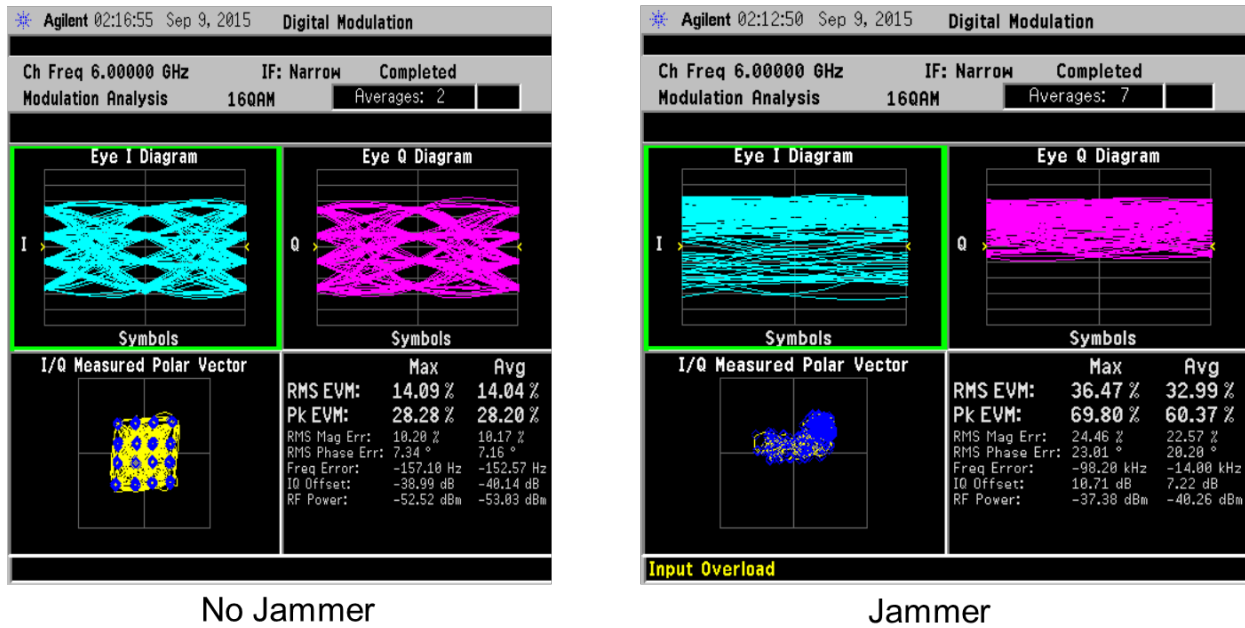
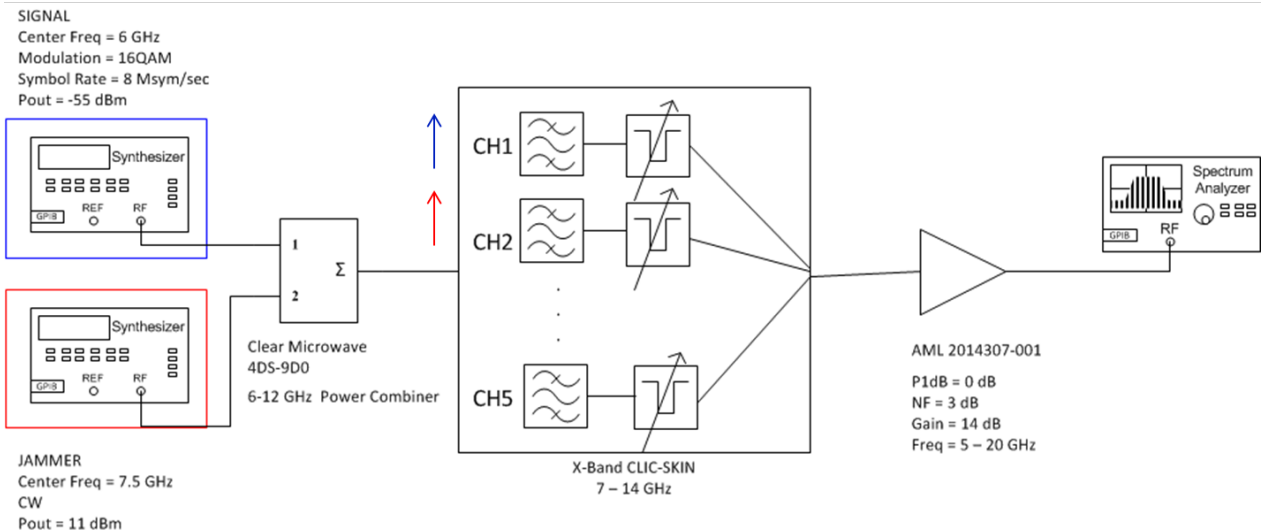


Figure 56. Response of the receiver before and after a close in jammer is presented.

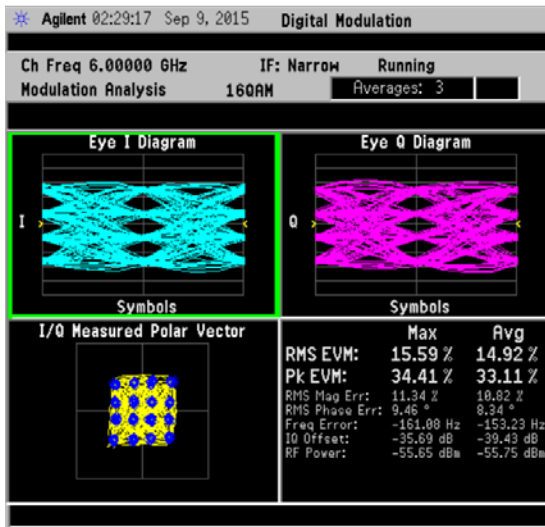
## Case 3 – Channelized Front End – Jammer Out of Band



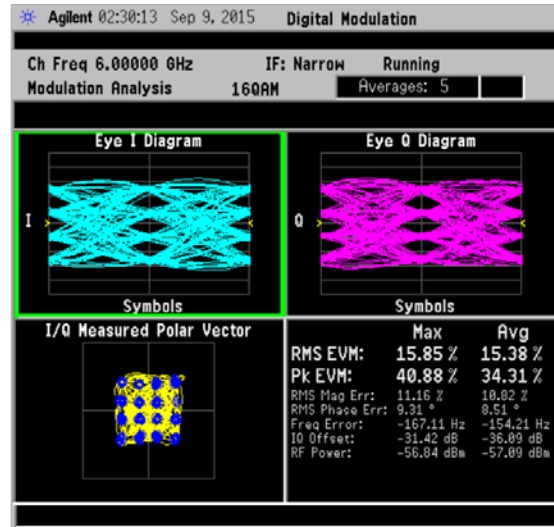
J/S Ratio: 66 dB

Figure 57. Test case for channelized RF front end.

### Case 3 – Channelized Front End – Jammer Out of Band



No Jammer



Jammer

Figure 58. Response of the receiver with channelization.

## REFERENCES

1. Gomez-Garcia, R., J. P. Magalhães, J. Muñoz-Ferreras, J. M. N. Vieira, N. Carvalho, and J. Pawlan. 2014. "Filling the Spectral Holes: Novel/Future Wireless Communications and Radar Receiver Architectures," *IEEE Microwave Magazine* 15(2):45–46.
2. Rauscher, C. 1994. "Efficient Design Methodology for Microwave Frequency Multiplexers Using Infinite-array Prototype Circuits," *IEEE Transactions on Microwave Theory and Techniques* 42(7):1337–1346.
3. Rauscher, C., J. M. Pond, and G. B. Tait. 1996. "Cryogenic Microwave Channelized Receiver," *IEEE Transactions on Microwave Theory and Techniques* 44(7):1240–1247.
4. Galbraith, C. J., R. D. White, C. Lei, K. Grosh, and G. M. Rebeiz. 2008. "Cochlea-based RF Channelizing Filters," *IEEE Transactions on Circuits and Systems I: Regular Papers* 55(4):969–979.
5. Jachowski, D. R. 2004. "Passive Enhancement of Resonator Q In Microwave Notch Filters." *2004 IEEE MTT-S International Microwave Symposium Digest* (pp. 1315–1318). June 6–11, Fort Worth, TX.
6. Jachowski, D. R. and A. C. Guyette. 2009. "Sub-octave-tunable Microstrip Notch Filter." *IEEE International Symposium on Electromagnetic Compatibility, 2009. EMC 2009* (pp. 99–102). August 17–21, Austin, TX.
7. Guyette, A. C., I. C. Hunter, and R. D. Pollard. 2009. "Design of Absorptive Microwave Filters Using Allpass Networks in a Parallel-cascade Configuration." *IEEE MTT-S International Microwave Symposium Digest, 2009. MTT '09* (pp. 733–736). June 7–12, Boston, MA.
8. Jachowski, D. R. 2012. "Octave Tunable Lumped-element Notch Filter." *2012 IEEE MTT-S International Microwave Symposium Digest (MTT)* (pp. 1–3). June 17–22, Montreal, QC, Canada.
9. Jachowski, D. R. 2005. "Compact, Frequency-agile, Absorptive Bandstop Filters." *2005 IEEE MTT-S International Microwave Symposium Digest* (pp. 4). June 17, Long Beach, CA.
10. Jachowski, D. R. and C. Rauscher. 2009. "Frequency-agile Bandstop Filter with Tunable Attenuation." *IEEE MTT-S International Microwave Symposium Digest MTT '09* (pp. 649–652), June 7–12, Boston, MA.
11. Jachowski, D. R. 2010. "Tunable Lumped-element Notch Filter with Constant Bandwidth." *2010 IEEE International Conference on Wireless Information Technology and Systems (ICWITS)* (pp. 1–4). August 28–September 3, Honolulu, HI.
12. Lee, J., T. C. Lee, and W. J. Chappell. 2012. "Lumped-element Realization of Absorptive Bandstop Filter with Anomalously High Spectral Isolation," *IEEE Transactions on Microwave Theory and Techniques* 60(8):2424–2430.
13. Rauscher, C. 1994. "Efficient Design Methodology for Microwave Frequency Multiplexers Using Infinite-Array Prototype Circuits," *IEEE Transactions on Microwave Theory and Techniques* 42(7):1337–1346.
14. Rauscher, C., J. M. Pond, and G. B. Tait. 1996. "Cryogenic Microwave Channelized Receiver," *IEEE Transactions on Microwave Theory and Techniques* 44(7):1240–1247.
15. Galbraith, C. J. and G. M. Rebeiz. 2008. "Higher Order Cochlea-like Channelizing Filters," *IEEE Transactions on Microwave Theory and Techniques* 56(7):1675–1683.
16. Ou, Y., G. M. Rebeiz. 2010. "A 20–90 MHz 26-channel Cochlear-based Channelizer." *2010 IEEE MTT-S International Microwave Symposium Digest (MTT)* (pp. 213–216). May 23–28, Anaheim, CA.
17. O'Brient, R. P. Ade, K. Arnold, J. Edwards, G. Engargiola, W. Holzapfel, A. T. Lee, M. Myers, G. Rebeiz, P. Richards, and A. Suzuki. 2011. "A Log-periodic Channelizer for Multichroic Antenna-coupled TES-Bolometers," *IEEE Transactions on Applied Superconductivity* 21(3):180–183.
18. Bevilacqua, A., A. Maniero, A. Gerosa, and A. Neviani. 2007. "An Integrated Solution for Suppressing WLAN Signals in UWB Receivers," *IEEE Transactions on Circuits and Systems I: Regular Papers* 54(8):1617–1625.

19. Luo, X., J. Ma, K. Ma, and K. S. Yeo. 2010. "Compact UWB Bandpass Filter with Ultra Narrow Notched Band," *IEEE Microwave and Wireless Components Letters* 20(3):145–147.
20. Liu, X., L. P. B. Katehi, W. J. Chappell, and D. Peroulis. 2009. "A 3.4–6.2 GHz Continuously Tunable Electrostatic MEMS Resonator with Quality Factor of 460–530." *2009 IEEE MTT-S International Microwave Symposium Digest* (pp. 1149–1152). June 7–12, Boston, MA.
21. Bode, H. W. 1935. "Wave Filter." U.S. Patent 2,002,216 (May). United States Patent and Trademark Office (USPTO), Alexandria, VA.
22. Cameron, R. I. and M. Yu. 2007. "Design of Manifold-coupled Multiplexers," *IEEE Microwave Magazine* 8(5):46–59.
23. Galbraith, C. J., R. D. White, L. Cheng, K. Grosh, and G. M. Rebeiz. 2008. "Cochlea-based RF Channelizing Filters," *IEEE Transactions on Circuits and Systems I: Regular Papers* 55(4):969–979.
24. Galbraith, C. J. and G. M. Rebeiz. 2008. "Higher Order Cochlea-like Channelizing Filters," *IEEE Transactions on Microwave Theory and Techniques* 56(7):1675–1683.
25. Magalhães, J. P., J.M.N. Vieira, R. Gomez-Garcia, and N. B. Carvalho. 2013. "Bio-inspired Hybrid Filter Bank for Software-defined Radio Receivers," *IEEE Transactions on Microwave Theory and Techniques* 61(4):1455–1466.
26. Galbraith, C., G. M. Rebeiz, and R. Drangmeister. 2007. "A Cochlea-based Preselector for UWB Applications." *2007 IEEE Radio Frequency Integrated Circuits (RFIC) Symposium* (pp. 219–222 ). June 3–5, Honolulu, HI.
27. Ye, S. and R. R. Mansour. 1994. "Design of Manifold-coupled Multiplexers Using Superconductive Lumped Element Filters." *1994 IEEE MTT-S International Microwave Symposium Digest* (pp.191–194). May 23–27, San Diego, CA.
28. Ou, Y. and G. M. Rebeiz. 2011. "Lumped Element Fully Tunable Bandstop Filters for Cognitive Radio Applications," *IEEE Transactions on Microwave Theory and Techniques* 59(10):2461–2468.
29. Jachowski, D. R. 2004. "Passive Enhancement of Resonator Q in Microwave Notch Filters." *2004 IEEE MTT-S International Microwave Symposium Digest* (pp. 13 15–13 18). June 6–11, Fort Worth, TX.
30. Guyette, A. C., I. C. Hunter, R. D. Pollard, and D. R. Jachowski. 2005. "Perfectly-matched Bandstop Filters Using Lossy Resonators." *IEEE MTT-S International Microwave Symposium Digest, 2005* (p. 4). June 17, Long Beach, CA.
31. Lee, T., J. Lee, E. J. Naglich, and D. Peroulis. 2014. "Octave Tunable Lumped-element Notch Filter with Resonator-Q-independent Zero Reflection Coefficient." *2014 IEEE MTT-S International Microwave Symposium (IMS)* (pp. 1–4). June 1–6, Tampa, FL.
32. Morgan, M. A. and T. A. Boyd. 2011. "Theoretical and Experimental Study of a New Class of Reflectionless Filter," *IEEE Transactions on Microwave Theory and Techniques* 59(5):1214–1221.
33. Shao, J. and Y. Lin. 2014. "Millimeter-wave Bandstop Filter with Absorptive Stopband." *2014 IEEE MTT-S International Microwave Symposium (IMS2014)* (pp. 1–4). June 1–6, Tampa, FL.
34. Bell, H. C. 1996. "L-resonator Bandstop Filters," *1996 IEEE Transactions on Microwave Theory and Techniques* 44(12):2669–2672.
35. Matthaei, G. L., L. Young, and E. M. T. Jones. 1980. *Microwave Filters, Impedance-matching Networks, and Coupling Structures*. Artech House, Inc., Norwood, MA.
36. Hong, J. and M. J. Lancaster. 2001. *Microstrip Filters for RF/Microwave Applications*. Wiley-Interscience, Hoboken, NJ.
37. Malherbe, J. A. G. and A. Swiatko. 2010. "Modified Chebyshev Bandstop Filter with Transmission Zeros at Real Frequencies," *Microwave and Optical Technology Letters* 53(1):177–180.
38. Woo, D., T. Lee, J. Lee, C. Pyo, and W. Choi. 2006. "Novel U-slot and V-slot DGSs for Bandstop Filter with Improved Q Factor," *IEEE Transactions on Microwave Theory and Techniques* 54(6):2840–2847.
39. Lee, J., E. J. Naglich, and W. J. Chappell. 2010. "Frequency Response Control in Frequency-agile Bandstop Filters," *IEEE Microwave and Wireless Components Letters* 20(12):669–671.

40. Kim, B., J. Lee, J. Lee, B. Jung, and W. J. Chappell. 2013. "RF CMOS Integrated On-chip Tunable Absorptive Bandstop Filter Using Qtunable Resonators," *IEEE Transactions on Electron Devices* 60(5): 1730–1737.
41. Bode, H. W. 1936. "Wave Filter." U.S. Patent 2,035,258 (March). United States Patent and Trademark Office (USPTO), Alexandria, VA.
42. Minasian, R. A., K. E. Alameh, and E. H. W. Chan. 2001. "Photonics-based Interference Mitigation Filters," *IEEE Transactions on Microwave Theory and Techniques* 49(10):1894–1899.
43. Marpaung, D., B. Morrison, R. Pant, and B. J. Eggleton. 2013. "Frequency Agile Microwave Photonic Notch Filter with Anomalously High Stopband Rejection," *Optics Letters* 38(21):4300–4303.
44. Marpaung, D., B. Morrison, R. Pant, C. Roeloffzen, A. Leinse, M. Hoekman, R. Heideman, and B. J. Eggleton. 2014. "Ultrahigh Suppression and Reconfigurable RF Photonic Notch Filter Using a Silicon Nitride Ring Resonator." *2014 Conference on Lasers and Electro-Optics (CLEO)*, (pp. 1-2, 8-13) June 8–13, San Jose, CA.
45. D. Marpaung, B. Morrison, R. Pant, C. Roeloffzen, A. Leinse, M. Hoekman, R. Heideman, and B. J. Eggleton. 2013. " $\text{Si}_3\text{N}_4$  Ring Resonator-based Microwave Photonic Notch Filter with an Ultrahigh Peak Rejection," *Optics Express* 21(20):23286–23294.
46. Matsko, A. B., W. Liang, A. Savchenkov, V. Ilchenko, D. Seidel, and L. Maleki. 2012. "Multi-octave Tunable Agile RF Photonic Filters." *2012 IEEE International Topical Meeting on Microwave Photonics (MWP)* (pp. 6–9). September 11–14, Noordwijk, Netherlands.
47. Naglich, E. J. and A. C. Guyette. 2016. "Frequency-selective Limiters Utilizing Contiguous-channel Double Multiplexer Topology," *IEEE Transactions on Microwave Theory and Techniques* 64(9):2871–2882.
48. Phudpong, P. and I. C. Hunter. 2008. "Frequency-selective Limiters Using Nonlinear Bandstop Filters," *IEEE Transactions on Microwave Theory and Techniques* 57(1):157–164.



REPORT DOCUMENTATION PAGE				Form Approved OMB No. 0704-01-0188	
<p>The public reporting burden for this collection of information is estimated to average 1 hour per response, including the time for reviewing instructions, searching existing data sources, gathering and maintaining the data needed, and completing and reviewing the collection of information. Send comments regarding this burden estimate or any other aspect of this collection of information, including suggestions for reducing the burden to Department of Defense, Washington Headquarters Services Directorate for Information Operations and Reports (0704-0188), 1215 Jefferson Davis Highway, Suite 1204, Arlington VA 22202-4302. Respondents should be aware that notwithstanding any other provision of law, no person shall be subject to any penalty for failing to comply with a collection of information if it does not display a currently valid OMB control number.</p> <p><b>PLEASE DO NOT RETURN YOUR FORM TO THE ABOVE ADDRESS.</b></p>					
<b>1. REPORT DATE (DD-MM-YYYY)</b>		<b>2. REPORT TYPE</b>		<b>3. DATES COVERED (From - To)</b>	
October 2017		Final			
<b>4. TITLE AND SUBTITLE</b>				<b>5a. CONTRACT NUMBER</b>	
Development of a Comb Limiter Combiner with Sub-band Known Interference Cancellation					
				<b>5b. GRANT NUMBER</b>	
				<b>5c. PROGRAM ELEMENT NUMBER</b>	
<b>6. AUTHORS</b>				<b>5d. PROJECT NUMBER</b>	
Jia-Chi Samuel Chieh					
				<b>5e. TASK NUMBER</b>	
				<b>5f. WORK UNIT NUMBER</b>	
<b>7. PERFORMING ORGANIZATION NAME(S) AND ADDRESS(ES)</b>				<b>8. PERFORMING ORGANIZATION REPORT NUMBER</b>	
SSC Pacific 53560 Hull Street San Diego, CA 92152-5001				TD 3324	
<b>9. SPONSORING/MONITORING AGENCY NAME(S) AND ADDRESS(ES)</b>				<b>10. SPONSOR/MONITOR'S ACRONYM(S)</b>	
Office of Naval Research 875 N. Randolph Street Arlington, VA 22203-1995				ONR	
				<b>11. SPONSOR/MONITOR'S REPORT NUMBER(S)</b>	
<b>12. DISTRIBUTION/AVAILABILITY STATEMENT</b>					
Approved for public release.					
<b>13. SUPPLEMENTARY NOTES</b>					
This is work of the United States Government and therefore is not copyrighted. This work may be copied and disseminated without restriction.					
<b>14. ABSTRACT</b>					
<p>The Navy is interested in anti-jam capabilities for bent-pipe satellite communication (SATCOM) systems. Legacy systems that receive substantial use include Commercial Wideband Satellite Program (CWSP), which has link allocations in the C-band uplink (3.7-4.2 GHz) and downlink (5.85-6.42 GHz), Defense Satellite Communication System (DSCS), and Wideband Global SATCOM (WGS), which both have link allocations in the X/Ku-bands uplink (7.9-8.4 GHz) and downlink (7.25-7.75 GHz). All of these systems provide essential coverage to the warfighter on land, ocean, and air; however, these bent-pipe SATCOM links are susceptible to jamming by an interferer, leading to denial of service. These systems have built-in interference mitigation techniques that include: frequency multiplexing, the use of guard bands to control emissions, and frequency hopping.</p> <p>Wideband SATCOM systems are desirable to support high throughput links but are particularly susceptible to jamming by an interferer. For example, wideband radio frequency (RF) front ends often employ a broadband low-noise amplifier (LNA). If the LNA receives a strong signal that is not the signal of interest (SOI) it can cause the amplifier to go into compression and become saturated. For wideband systems this becomes especially serious because the likelihood of spurious signals increases. One method to mitigate this effect is to frequency multiplex the bandwidth of interest, essentially channelizing the spectrum. Although frequency multiplexing the full spectrum into subchannels localizes failure to a subchannel, loss of a subchannel can still have tremendous repercussions depending on the subchannel bandwidth. Therefore, the ability to mitigate interferer signals is essential.</p>					
<b>15. SUBJECT TERMS</b>					
anti-jam capabilities; bent-pipe satellite communication; Commercial Wideband Satellite Program; Defense Satellite Communication System; Wideband Global SATCOM; spurious signals; cochlea-based channelizer; frequency agile absorptive notch filters;					
<b>16. SECURITY CLASSIFICATION OF:</b>			<b>17. LIMITATION OF ABSTRACT</b>	<b>18. NUMBER OF PAGES</b>	<b>19a. NAME OF RESPONSIBLE PERSON</b>
<b>a. REPORT</b>	<b>b. ABSTRACT</b>	<b>c. THIS PAGE</b>			Jia-Chi Samuel Chieh
U	U	U	U	55	<b>19b. TELEPHONE NUMBER (Include area code)</b> (619)553-6404

## INITIAL DISTRIBUTION

84300	Library	(1)
85300	Archive/Stock	(1)
55250	J. Chieh	(1)

Defense Technical Information Center Fort Belvoir, VA 22060-6218	(1)
---	-----

Approved for public release.



SSC Pacific  
San Diego, CA 92152-5001